Chemistry of *C*-Trimethylsilyl-Substituted Heterocarboranes. 15. Synthetic, Spectroscopic, Reactivity, and Bonding Studies on the "Carbons Apart" *closo*-1-Sn-2-($SiMe_3$)-4-(R)-2,4-$C_2B_4H_4$: Crystal Structures of the Donor–Acceptor Complexes 1-Sn(L)-2,4-($SiMe_3$)$_2$-2,4-$C_2B_4H_4$ [R = $SiMe_3$, Me; L = 2,2′-$C_{10}H_8N_2$, 2,2′-$C_8H_6N_4$, or (η^5-C_5H_5)Fe(η^5-$C_5H_4CH_2(Me)_2N$)]†

Narayan S. Hosmane,* Lei Jia, Hongming Zhang, and John A. Maguire

Department of Chemistry, Southern Methodist University, Dallas, Texas 75275

Received December 7, 1993®

The reactions of the THF-solvated "*carbons apart*" disodium compounds, *closo-exo*-5,6-Na(THF)$_2$-1-Na(THF)$_2$-2-($SiMe_3$)-4-(R)-2,4-$C_2B_4H_4$ (R = $SiMe_3$, Me), with anhydrous $SnCl_2$ in THF in molar ratios of 1:1 at 0 °C produced the corresponding *closo*-stannacarboranes, 1-Sn-2,4-($SiMe_3$)$_2$-2,4-$C_2B_4H_4$ (**I**) and 1-Sn-2-($SiMe_3$)-4-(Me)-2,4-$C_2B_4H_4$ (**II**), as colorless liquids in 86 and 51% yields, respectively. The *closo*-stannacarboranes react with 2,2′-bipyridine, 2,2′-bipyrimidine, (ferrocenylmethyl)-*N*,*N*-dimethylamine, and 2,2′:6′,2″-terpyridine in benzene at room temperature to form the corresponding donor–acceptor complexes, 1-Sn($C_{10}H_8N_2$)-2,4-($SiMe_3$)$_2$-2,4-$C_2B_4H_4$ (**III**), 1-Sn($C_8H_6N_4$)-2,4-($SiMe_3$)$_2$-2,4-$C_2B_4H_4$ (**IV**), 1-Sn($C_8H_6N_4$)-2-($SiMe_3$)-4-(Me)-2,4-$C_2B_4H_4$ (**V**), 1-Sn[(η^5-C_5H_5)Fe(η^5-$C_5H_4CH_2(Me)_2N$)]-2,4-($SiMe_3$)$_2$-2,4-$C_2B_4H_4$ (**VI**), 1-Sn[(η^5-C_5H_5)Fe(η^5-$C_5H_4CH_2(Me)_2N$)]-2-($SiMe_3$)-4-(Me)-2,4-$C_2B_4H_4$ (**VII**), and 1-Sn($C_{15}H_{11}N_3$)-2,4-($SiMe_3$)$_2$-2,4-$C_2B_4H_4$ (**VIII**), in 62–95% yields. The complexes **I**–**VIII** were all characterized on the basis of ^1H, ^{11}B, ^{13}C, and ^{119}Sn NMR spectra and IR and mass spectra. The mass spectra of donor–acceptor complexes show only groupings corresponding to their stannacarborane and base fragments rather than the molecular ions. The complexes **III**, **IV**, and **VI** were also characterized by single crystal X-ray analyses. The crystal structures show that each complex has a distorted pentagonal bipyramidal geometry with the capping tin metal coordinating to the nitrogen atom(s) of the respective Lewis base, in a manner similar to that found in the corresponding "*carbons adjacent*" isomers. However, the geometries of the donor–acceptor complexes in the two carborane systems are quite different. The structures of **I** and **III** were analyzed using MNDO and Fenske–Hall molecular orbital calculations. The donor–acceptor complexes **III**, **IV**, and **VI** all crystallized in the monoclinic space group $P2_1/c$ with a = 6.807(1), 10.887(2), and 6.518(2) Å, b = 18.841(5), 19.472(5), and 39.56(1) Å, c = 19.513(4), 11.661(3), and 11.192(4) Å, β = 96.82(2), 97.89(2), and 93.81(3)°, V = 2484.8(9), 2449(1), and 2879(2) Å^3 and Z = 4, 4, and 4, respectively. The final refinements of **III**, **IV**, and **VI** converged at R = 0.028, 0.031, and 0.033 and R_w = 0.038, 0.046, and 0.039, respectively.

Introduction

The chemistry of the group 14 metallacarboranes has received much attention in recent years.[1,2] In particular, the Lewis acid–base chemistry of the pentagonal bipyramidal, "*carbons adjacent*" stanna-, germa-, and plumbacarboranes of the type 1-(M)-2-($SiMe_3$)-3-(R)-2,3-$C_2B_4H_4$ (M = Sn, Ge, or Pb; R = $SiMe_3$, Me, or H) has been investigated and the structures of the resulting donor–acceptor complexes involving Lewis bases, such as 2,2′-bipyridine, 1,10-phenanthroline, 2,2′-bipyrimidine, (ferrocenylmethyl)-*N*,*N*-dimethylamine (ferrocene amine), and 2,2′:6′,2″-terpyridine, have been reported.[3–6] The structures of these complexes show that the group 14 metal

† Taken in part from the M.S. Thesis of Mr. Lei Jia, Southern Methodist University, Dallas, Texas, 1992.

® Abstract published in *Advance ACS Abstracts*, March 1, 1994.

(1) (a) Hosmane, N. S.; Maguire, J. A. In *Advances in Boron and the Boranes*; Liebman, J. F., Greenberg, A., Williams, R. E., Eds.; Molecular Structure and Energetics; VCH: New York, 1988; Vol. 5, Chapter 14, p 297. (b) Hosmane, N. S.; Maguire, J. A. *Adv. Organomet. Chem.* **1990**, *30*, 99.

(2) (a) Hosmane, N. S.; Maguire, J. A. In *Electron Deficient Boron and Carbon Clusters*; Olah, G. A., Wade, K., Williams, R. E., Eds.; Wiley: New York, 1991; Chapter 9, p 215. (b) Hosmane, N. S. *Pure Appl. Chem.* **1991**, *63*, 375. (c) Hosmane, N. S.; Maguire, J. A. *J. Cluster Sci.* **1993**, *4*, 297. (d) Saxena, A. K.; Maguire, J. A.; Banewicz, J. J.; Hosmane, N. S. *Main Group Chem. News* **1993**, *1*, 14.

(3) (a) Cowley, A. H.; Galow, P.; Hosmane, N. S.; Jutzi, P.; Norman, N. C. *J. Chem. Soc., Chem. Commun.* **1984**, 1564. (b) Hosmane, N. S.; de Meester, P.; Maldar, N. N.; Potts, S. B.; Chu, S. S. C.; Herber, R. H. *Organometallics* **1986**, *5*, 772. (c) Siriwardane, U.; Hosmane, N. S.; Chu, S. S. C. *Acta Crystallogr., Cryst. Struct. Commun.* **1987**, *C43*, 1067. (d) Hosmane, N. S.; Islam, M. S.; Siriwardane, U.; Maguire, J. A.; Campana, C. F. *Organometallics* **1987**, *6*, 2447. (e) Siriwardane, U.; Hosmane, N. S. *Acta Crystallogr., Cryst. Struct. Commun.* **1988**, *C44*, 1572. (f) Hosmane, N. S.; Fagner, J. S.; Zhu, H.; Siriwardane, U.; Maguire, J. A.; Zhang, G.; Pinkston, B. S. *Organometallics* **1989**, *8*, 1769. (g) Siriwardane, U.; Maguire, J. A.; Banewicz, J. J.; Hosmane, N. S. *Organometallics* **1989**, *8*, 2792. (h) Hosmane, N. S.; Barreto, R. D.; Tolle, M. A.; Alexander, J. J.; Quintana, W.; Siriwardane, U.; Shore, S. G.; Williams, R. E. *Inorg. Chem.* **1990**, *29*, 2698. (i) Maguire, J. A.; Fagner, J. S.; Siriwardane, U.; Banewicz, J. J.; Hosmane, N. S. *Struct. Chem.* **1990**, *1*, 583.

(4) (a) Hosmane, N. S.; Siriwardane, U.; Islam, M. S.; Maguire, J. A.; Chu, S. S. C. *Inorg. Chem.* **1987**, *26*, 3428. (b) Hosmane, N. S.; Islam, M. S.; Pinkston, B. S.; Siriwardane, U.; Banewicz, J. J.; Maguire, J. A. *Organometallics* **1988**, *7*, 2340.

0276-7333/94/2313-1411$04.50/0

acts as the acid site in bonding to the base. Coordination by the base leads to a distortion of the MC_2B_4 cage in that the metal atom is dislocated, or slipped, toward the boron side of the C_2B_3 face of the carborane. In all cases the base molecules are oriented opposite the cage carbons. The structures of base–stannacarborane complexes in the larger cage icosahedral system show similar distortions and base orientations.[7] In contrast, very little information is available on the corresponding "*carbons apart*" metallacarboranes; no structures have been reported for any group 14 metallacarborane, based on either the C_2B_4 or C_2B_9 carbons apart carborane ligands.[1,2] One of the main factors limiting the study of these metallacarboranes has been the lack of a reliable synthetic route to the carbons apart isomers. However, the recent reports on the syntheses and crystal structures of the disodium and dilithium compounds, *closo-exo*-5,6-M(solv)$_n$-1-M(solv)$_n$-2-($SiMe_3$)-4-(R)-2,4-$C_2B_4H_4$ (R = $SiMe_3$, Me; n = 1, solv = THF or TMEDA, M = Li or Na; n = 2, solv = THF, M = Na),[8] describe a convenient synthesis for these synthons and open up a number of possibilities for the synthesis of metallacarboranes that may have chemical and physical properties different from those of their better known carbons adjacent analogues. As part of our investigation of the reaction chemistry of the carbons apart group 1 metallacarboranes, we have investigated the reactivity of the THF-solvated disodium compound toward $SnCl_2$, and report herein the details of these studies and characterization of their product *closo*-stannacarboranes. The reactivities of these stannacarboranes toward monodentate, bidentate, bis(bidentate), and tridentate Lewis bases are also reported, along with the spectroscopic characterizations and the results of X-ray diffraction studies of several of the resulting donor–acceptor complexes.

Experimental Section

Materials. 1,2-Bis(trimethylsilyl)-1,2-dicarba-*closo*-hexaborane(6), and 1-(trimethylsilyl)-2-methyl-1,2-dicarba-*closo*-hexaborane(6) were prepared and converted to their corresponding tetrahydrofuran (THF)-solvated carbons apart natracarboranes, *closo-exo*-5,6-Na(THF)$_2$-1-Na(THF)$_2$-2-($SiMe_3$)-4-(R)-2,4-$C_2B_4H_4$ (R = $SiMe_3$, Me), using the method described in the literature.[3h,8,9] Before use, naphthalene (Aldrich), 2,2′-bipyridine (Aldrich), 2,2′-bipyrimidine (Lancaster Syntheses), and 2,2′:6′,2″-terpyridine (Aldrich) were sublimed *in vacuo* and their purity was checked by IR and NMR spectra and melting point measurements. Sodium metal (Aldrich) was freshly cut in a drybox, (ferrocenylmethyl)-*N*,*N*-dimethylamine (Strem Chemicals, Inc.) was distilled *in vacuo*, and $SnCl_2$ (Strem Chemicals, Inc.) was dried *in vacuo* by heating at 110 °C overnight. Benzene, THF, and *n*-hexane were dried over $LiAlH_4$ and doubly distilled; all other solvents were dried over 4–8-mesh molecular sieves (Aldrich) and either saturated with dry argon or degassed before use.

Spectroscopic and Analytical Procedures. Proton, boron-11, carbon-13, and tin-119 pulse Fourier transform NMR spectra, at 200, 64.2, 50.3, and 74.63 MHz, respectively, were recorded on an IBM-WP200 SY multinuclear NMR spectrometer. Infrared spectra were recorded on a Perkin-Elmer Model 283 infrared spectrophotometer and a Perkin-Elmer Model 1600 FT-IR spectrophotometer. Mass spectral determinations were performed at the Midwest Center for Mass Spectrometry, University of Nebraska—Lincoln, Nebraska. Elemental analyses were obtained from Oneida Research Services (ORS) Inc., Whitesboro, NY.

Synthetic Procedures. All experiments were carried out in Pyrex glass round bottom flasks of 250-mL capacity, containing magnetic stirring bars and fitted with high-vacuum Teflon valves. Nonvolatile substances were manipulated in either a drybox or evacuable glovebags under an atmosphere of dry nitrogen. All known compounds among the products were identified by comparing their IR and NMR spectra with those of the authentic samples.

Synthesis of *closo*-1-Sn-2,4-($SiMe_3$)$_2$-2,4-$C_2B_4H_4$ (I) and *closo*-1-Sn-2-($SiMe_3$)-4-(Me)-2,4-$C_2B_4H_4$ (II). A 5.87-mmol (3.238-g) crystalline sample of *closo-exo*-5,6-Na(THF)$_2$-1-Na(THF)$_2$-2,4-($SiMe_3$)$_2$-2,4-$C_2B_4H_4$ [prepared from *closo*-1,2-($SiMe_3$)$_2$-1,2-$C_2B_4H_4$ (1.31 g, 6.02 mmol), freshly cut sodium metal (0.28 g, 12.18 mmol), and naphthalene (1.56 g, 12.17 mmol) as described elsewhere][8] or a 6.87-mmol (3.391-g) crystalline sample of *closo-exo*-5,6-Na(THF)$_2$-1-Na(THF)$_2$-2-($SiMe_3$)-4-(Me)-2,4-$C_2B_4H_4$ [prepared similarly from *closo*-1-($SiMe_3$)-2-(Me)-1,2-$C_2B_4H_4$ (1.13 g, 7.08 mmol), freshly cut sodium metal (0.34 g, 14.79 mmol), and naphthalene (1.91 g, 14.90 mmol)][8] was dissolved in 15 mL of anhydrous THF *in vacuo*. This solution was slowly poured *in vacuo* onto the anhydrous $SnCl_2$ (1.113 g, 5.87 mmol or 1.303 g, 6.87 mmol) at 0 °C, and the resulting brown heterogeneous mixture was stirred constantly at this temperature for 4 h, during which time the solution turned black. The solvent, THF, was then removed at this temperature via vacuum distillation over a period of 2 h, and the reaction flask containing the dark brown residue was attached to a detachable U-trap that was immersed in an ice bath. After the dark brown residue was heated in the flask to 100 °C by using an oil bath, a colorless liquid, identified as *closo*-1-Sn-2,4-($SiMe_3$)$_2$-2,4-$C_2B_4H_4$ (I) (1.69 g, 5.02 mmol, 86% yield, bp 125 °C at 10^{-4} Torr) or another colorless liquid, identified as *closo*-1-Sn-2-($SiMe_3$)-4-(Me)-2,4-$C_2B_4H_4$ (II) (0.98 g, 3.52 mmol, 51% yield, 113 °C at 10^{-4} Torr), was collected in the detachable U-trap at 0 °C. The side arms of both the reaction flask and the U-trap were maintained at ~100 °C with heating tape during the distillation of the product. A black residue that remained at the bottom of the reaction flask after distillation was found to be insoluble in both polar and nonpolar organic solvents and, therefore, was discarded. Both **I** and **II** are slightly sensitive to air and moisture and are highly soluble in both polar and nonpolar organic solvents. Anal. Calcd for $C_8H_{22}B_4Si_2Sn$ (I) and $C_6H_{16}B_4SiSn$ (II): C, 28.51 and 25.84; H, 6.53 and 5.74; Sn, 35.25 and 42.59. Found: C, 28.67 and 25.98; H, 6.63 and 5.77; Sn, 35.12 and 42.31. Mass spectral analyses (HREI): theoretical mass for the parent ion groupings of **I**, $[^{12}C_8{}^1H_{22}{}^{10}B^{11}B_3{}^{28}Si_2{}^{118}Sn]^+$ and $[^{12}C_8{}^1H_{22}{}^{10}B^{11}B_3{}^{28}Si_2{}^{116}Sn]^+$, m/z 335.0702 and 333.0705; measured mass m/z 335.0688 and 333.0701. Mass spectral analyses (HREI): theoretical mass for the parent ion groupings of **II**, $[^{12}C_6{}^1H_{16}{}^{11}B_4{}^{28}Si^{119}Sn]^+$, $[^{12}C_6{}^1H_{16}{}^{11}B_4{}^{28}Si^{118}Sn]^+$, $[^{12}C_5{}^1H_{13}{}^{11}B_4{}^{28}Si^{119}Sn]^+$, and $[^{12}C_5{}^1H_{13}{}^{11}B_4{}^{28}Si^{118}Sn]^+$, m/z 279.0428, 278.0412, 264.0181, and 263.0157; measured mass m/z 279.0430, 278.0420, 264.0194, and 263.0157. The NMR and IR spectral data of **I** and **II** are given in Tables 5 and 6.

Synthesis of 1-Sn($C_{10}H_8N_2$)-2,4-($SiMe_3$)$_2$-2,4-$C_2B_4H_4$ (III). A clear, colorless solution of 1-Sn-2,4-($SiMe_3$)$_2$-2,4-$C_2B_4H_4$ (I) (0.84 g, 2.5 mmol) in freshly distilled dry benzene (10 mL) was added to a flask containing 2,2′-bipyridine, $C_{10}H_8N_2$ (0.39 g, 2.5

(5) (a) Hosmane, N. S.; Lu, K.-J.; Siriwardane, U.; Shet, M. S. *Organometallics* **1990**, *9*, 2798. (b) Hosmane, N. S.; Lu, K.-J.; Zhang, H.; Maguire, J. A.; Jia, L.; Barreto, R. D. *Organometallics* **1992**, *11*, 2458.

(6) (a) Hosmane, N. S.; Siriwardane, U.; Zhu, H.; Zhang, G.; Maguire, J. A. *Organometallics* **1989**, *8*, 566. (b) Hosmane, N. S.; Lu, K.-J.; Zhu, H.; Siriwardane, U.; Shet, M. S.; Maguire, J. A. *Organometallics* **1990**, *9*, 808. (c) Siriwardane, U.; Lu, K.-J.; Hosmane, N. S. *Acta Crystallogr., Cryst. Struct. Commun.* **1990**, *C46*, 1391. (d) Zhang, H.; Jia, L.; Hosmane, N. S. *Acta Crystallogr., Cryst. Struct. Commun.* **1993**, *C49*, 791.

(7) Jutzi, P.; Galow, P.; Abu-Orabi, S.; Arif, A. M.; Cowley, A. H.; Norman, N. C. *Organometallics* **1987**, *6*, 1024.

(8) (a) Zhang, H.; Wang, Y.; Saxena, A. K.; Oki, A. R.; Maguire, J. A.; Hosmane, N. S. *Organometallics* **1993**, *12*, 3933. (b) Hosmane, N. S.; Jia, L.; Zhang, H.; Bausch, J. W.; Prakash, G. K. S.; Williams, R. E.; Onak, T. P. *Inorg. Chem.* **1991**, *30*, 3793. (c) Jia, L. M.S. Thesis, Southern Methodist University, Dallas, Texas, 1992.

(9) Hosmane, N. S.; Saxena, A. K.; Barreto, R. D.; Zhang, H.; Maguire, J. A.; Jia, L.; Wang, Y.; Oki, A. R.; Grover, K. V.; Whitten, S. J.; Dawson, K.; Tolle, M. A.; Siriwardane, U.; Demissie, T.; Fagner, J. S. *Organometallics* **1993**, *12*, 3001.

mmol), in benzene (5 mL) at 0 °C. The resulting homogeneous solution turned orange brown almost immediately. This solution was constantly stirred for 24 h at room temperature, during which time it became turbid. Benzene was then removed from the solution *in vacuo*, and the resulting dark orange residue that remained in the flask was heated to 50 °C to collect unreacted 2,2′-bipyridine (0.03 g, 0.2 mmol) in a detachable U-trap at −78 °C. After complete removal of unreacted 2,2′-bipyridine, the flask containing the dark orange residue was attached to another detachable U-trap that was immersed in an ice bath. On heating the flask to 130–140 °C *in vacuo*, over a period of 10 h, a pale yellow crystalline solid, identified as **III**, was collected on the inside walls of the U-trap (1.09 g, 2.23 mmol, 89% yield, mp 87 °C) at 0 °C. The side arms of both the reaction flask and the U-trap were maintained at ~130 °C with heating tape during the sublimation of the product. The brown polymeric mass (not measured), which remained at the bottom of the reaction flask after sublimation, was found to be insoluble in both polar and nonpolar organic solvents and, therefore, was discarded. At room temperature, **III** is highly soluble in both polar and nonpolar organic solvents. Anal. Calcd for $C_{18}H_{30}N_2B_4Si_2Sn$ (**III**): C, 43.90; H, 6.14; N, 5.69; Sn, 24.10. Found: C, 44.67; H, 6.33; N, 6.12; Sn, 23.56. The low resolution electron impact (LREI) and low resolution fast atom bombardment (LRFAB) mass spectral analysis of **III** do not exhibit the molecular ion. However, the groupings with the major cutoffs at *m/z* 338, 323, and 156 corresponded to the fragments $^{120}Sn(^{12}CH_3)_6{}^{28}Si_2{}^{12}C_2{}^{11}B_4H_4^+$, $^{120}Sn(^{12}CH_3)_5{}^{28}Si_2{}^{12}C_2{}^{11}B_4H_4^+$, and $^{12}C_{10}H_8{}^{14}N_2^+$, respectively. The NMR and IR spectral data of **III** are given in Tables 5 and 6.

Synthesis of 1-Sn($C_8H_6N_4$)-2,4-($SiMe_3$)$_2$-2,4-$C_2B_4H_4$ (IV) and 1-Sn($C_8H_6N_4$)-2-($SiMe_3$)-4-(Me)-2,4-$C_2B_4H_4$ (V). In a procedure identical with that described for the synthesis of the carbons adjacent isomers,[3f] **I** (0.81 g, 2.4 mmol) and **II** (0.55 g, 1.98 mmol) were reacted, in separate experiments, with freshly sublimed 2,2′-bipyrimidine, $C_8H_6N_4$ (0.190 g, 1.2 mmol and 0.158 g, 1.0 mmol, respectively), in dry benzene (15 mL) at room temperature for 3 days. After removal of all the unreacted *closo*-stannacarborane precursors (**I**, 0.31 g, 0.90 mmol; **II**, 0.26 g, 0.93 mmol; collected in detachable U-traps held at 0 °C) by mild heating of the reaction residue at 80 °C, a reddish-brown solid remained in the flask which was then further heated to 125 °C to collect **IV** (0.46 g, 0.93 mmol, 62% yield based on **I** consumed, mp 126 °C) and **V** (0.36 g, 0.83 mmol, 79% yield based on **II** consumed, mp 109 °C) as sublimed orange crystalline products on the inside walls of the second U-traps at 0 °C, respectively. The yields of **IV** and **V** based on bipyrimidine used were 78% and 83%, respectively. A dark polymeric mass (not measured) that remained at the bottom of the reaction flask after sublimation was found to be insoluble in both polar and nonpolar organic solvents and, therefore, was discarded. At room temperature, both **IV** and **V** are highly soluble in polar and nonpolar organic solvents. Anal. Calcd for $C_{16}H_{28}N_4B_4Si_2Sn$ (**IV**) and $C_{14}H_{22}N_4B_4SiSn$ (**V**): C, 38.86 and 38.54; H, 5.71 and 5.08; N, 11.33 and 12.84. Found: C, 39.12 and 38.22; H, 5.91 and 5.32; N, 11.96 and 12.67. As in the case of **III**, the HREI, LREI, and LRFAB mass spectral analyses of **IV** and **V** do not exhibit the molecular ions; instead, the ions of their fragment stannacarborane precursors, **I** and **II**, and of 2,2′-bipyrimidine (*m/z* 158) were observed. The NMR and IR spectral data of **IV** and **V** are given in Tables 5 and 6.

Synthesis of 1-Sn[(η^5-C_5H_5)Fe(η^5-$C_5H_4CH_2(Me)_2N$)]-2,4-($SiMe_3$)$_2$-2,4-$C_2B_4H_4$ (VI) and 1-Sn[(η^5-C_5H_5)Fe(η^5-$C_5H_4CH_2(Me)_2N$)]-2-($SiMe_3$)-4-(Me)-2,4-$C_2B_4H_4$ (VII). In a procedure identical with that employed for the synthesis of carbons adjacent isomers,[3f] 1.50 mmol (0.505 g) of **I** or 1.65 mmol (0.46 g) of **II** was allowed to react with (ferrocenylmethyl)-*N*,*N*-dimethylamine, $C_{13}H_{17}NFe$ (0.37 g, 1.52 mmol or 0.41 g, 1.69 mmol), in dry benzene (15–20 mL) at room temperature for 5 days. After removal of benzene and a trace quantity of unreacted $C_{13}H_{17}NFe$ *in vacuo*, the dark orange residue in the flask was sublimed at 80 °C to collect orange crystals, identified as **VI** (0.76 g, 1.31 mmol, mp 48 °C) or **VII** (0.818 g, 1.57 mmol, 43 °C) in 87 or 95% yield. Complexes **VI** and **VII** are soluble in both polar and nonpolar organic solvents and were recrystallized from a benzene solution. Anal. Calcd for $C_{21}H_{39}NSi_2B_4FeSn{\cdot}C_6H_6$ (**VI**): C, 49.31; H, 6.90; N, 2.13. Found: C, 47.96; H, 6.97; N, 3.04. Calcd for $C_{19}H_{33}NSiB_4FeSn{\cdot}C_6H_6$ (**VII**): C, 50.09; H, 6.56; N, 2.34. Found: C, 48.90; H, 6.72; N, 2.81. As in the previous cases, the mass spectra failed to exhibit the parent ions; only the ion fragments of the reactants were observed. The NMR and IR spectral data of **VI** and **VII** are given in Tables 5 and 6.

Synthesis of 1-Sn($C_{15}H_{11}N_3$)-2,4-($SiMe_3$)$_2$-2,4-$C_2B_4H_4$ (VIII). In a procedure identical with that employed for the synthesis of the carbons adjacent isomer,[3g] 0.49 g (1.46 mmol) of **I** was reacted with freshly sublimed 0.34 g (1.46 mmol) of 2,2′:6′,2″-terpyridine in dry benzene (20 mL) at room temperature for 4 days to isolate 0.75 g (1.32 mmol) of a microcrystalline dark orange solid, identified as **VIII** (mp 130–132 °C), in 90% yield. Complex **VIII** is highly soluble in both polar and nonpolar organic solvents. Anal. Calcd for $C_{23}H_{33}N_3Si_2B_4Sn$ (**VIII**): C, 48.50; H, 5.84; N, 7.38. Found: C, 49.92; H, 6.01; N, 7.53. The mass spectrum of **VIII** failed to exhibit the parent ions; only the ion fragments of the reactants were observed. The NMR and IR spectral data of **VIII** are given in Tables 5 and 6.

X-ray Analyses of 1-Sn($C_{10}H_8N_2$)-2,4-($SiMe_3$)$_2$-2,4-$C_2B_4H_4$ (III), 1-Sn-($C_8H_6N_4$)-2,4-($SiMe_3$)$_2$-2,4-$C_2B_4H_4$ (IV), and 1-Sn-[(η^5-C_5H_5)Fe(η^5-$C_5H_4CH_2(Me)_2N$)]-2,4-($SiMe_3$)$_2$-2,4-$C_2B_4H_4$ (VI). Yellow crystals of **III** and orange crystals of **IV** and **VI** were grown by vacuum sublimation onto glass surfaces in 8-mm tubes. The crystals were all coated with an epoxy resin and mounted on a Siemens R3m/V diffractometer. Final unit cell parameters, given in Table 1, were obtained by least-squares fits of 24 accurately centered reflections, measured in the ranges 17° < 2θ < 29°, 17° < 2θ < 29°, and 15° < 2θ < 30° for **III**, **IV**, and **VI**, respectively; intensity data were collected on all three compounds at 230 K in the range 3.5° ≤ 2θ ≤ 42.0°. Three standard reflections, monitored after every 150 reflections, did not show any significant change in intensity during the data collection. The data were corrected for Lorentz and polarization effects, and semiempirical absorption corrections (based on ψ scans) were applied with the minimum and maximum transmission factors of 0.617 and 0.882, 0.700 and 0.981, and 0.685 and 0.920 for **III**, **IV**, and **VI**, respectively. The structures were solved by heavy-atom methods using the *SHELXTL-Plus* package.[10] Full-matrix least-squares refinements were performed. All non-H atoms were refined anisotropically. The scattering factors, with anomalous dispersion correction for heavy atoms, were taken from ref 11. Carborane cage H atoms were located in difference Fourier maps, while the remaining H's were placed in idealized positions with fixed isotropic temperature factors (U = 0.08 Å^2). The final cycles of refinement converged at R = 0.028, 0.031, and 0.033, R_w = 0.038, 0.046, and 0.039, and GOF = 1.38, 1.48, and 1.31 for **III**, **IV**, and **VI**, respectively. The final atomic coordinates are given in Table 2, selected bond lengths and bond angles are presented in Table 3, and selected mean deviations and dihedral angles of some important least-squares planes are given in Table 4.

Calculations. Molecular orbital calculations on **I** and **III** were carried out using the unparameterized Fenske–Hall method[12] and MNDO semiempirical molecular orbital theory.[13] The basis functions used in the Fenske–Hall calculations were those generated by the numerical Xα atomic orbital program of Herman and Skillman,[14] used in conjunction with the Xα-to-Slater

(10) Sheldrick, G. M. *Structure Determination Software Programs*; Siemens X-ray Analytical Instrument Corp.: Madison, WI, 1990.
(11) *International Tables For X-ray Crystallography*; Kynoch Press: Birmingham, U.K., 1974; Vol. IV.
(12) Hall, M. B.; Fenske, R. F. *Inorg. Chem.* **1972**, *11*, 808.
(13) Version 5.0 1 of the MOPAC package; see: Stewart, J. J. P. *QCPE Bull.* **1983**, *3*, 43.
(14) Herman, F.; Skillman, S. *Atomic Structure Calculations*, Prentice-Hall: Englewood Cliffs, NJ, 1963.

Table 1. Crystallographic Data[a] for III, IV, and VI

	III	IV	VI
formula	$C_{18}H_{30}N_2B_4Si_2Sn$	$C_{16}H_{28}N_4B_4Si_2Sn$	$C_{21}H_{39}NB_4Si_2FeSn$
fw	492.5	494.5	579.5
cryst syst	monoclinic	monoclinic	monoclinic
space group	$P2_1/c$	$P2_1/c$	$P2_1/c$
a, Å	6.807(1)	10.887(2)	6.518(2)
b, Å	18.841(5)	19.472(5)	39.559(11)
c, Å	19.513(4)	11.661(3)	11.192(4)
β, deg	96.82(2)	97.89(2)	93.81(3)
V, Å^3	2484.8(9)	2449(1)	2879(2)
Z	4	4	4
D_{calcd}, g cm^{-3}	1.317	1.341	1.337
cryst dmns, mm	0.30 × 0.20 × 0.15	0.25 × 0.10 × 0.35	0.25 × 0.35 × 0.15
scan type	$\omega/2\theta$	$\omega/2\theta$	$\omega/2\theta$
scan sp in ω; min, max	5.0, 25.0	5.0, 25.0	4.0, 20.0
2θ range, deg	3.5–42.0	3.5–42.0	3.5–42.0
no. of data collcd	3088	2921	3612
no. of ind data	2688	2636	3118
T, K	230	230	230
decay, %	0	0	0
no. of obsd reflctns, $I > 3.0\sigma(I)$	2172	2261	2160
no. of paramrs refined	244	244	271
GOF	1.38	1.48	1.31
R^b	0.028	0.031	0.033
R_w	0.038	0.046	0.039
$\Delta\rho$ (max, min), e/Å^3	0.38, –0.51	0.71, –0.62	0.32, –0.51
g^c	0.0004	0.0007	0.0003
abs coeff, mm^{-1}	1.131	1.150	1.465

[a] Graphite monochromatized Mo Kα radiation, λ = 0.710 73 Å. [b] $R = \sum||F_o| - |F_c||/\sum|F_o|$, $R_w = [\sum w(F_o - F_c)^2/\sum w(F_o)^2]^{1/2}$. [c] $w = 1/[\sigma^2(F_o) + g(F_o)^2]$.

program of Bursten and Fenske.[15] The MNDO parameters for carbon, boron, hydrogen, and silicon were those stored in version 5.01 of the MOPAC package,[13] while the tin parameters were those given by Dewar and co-workers.[16] The heavy-atom positions used in the Fenske–Hall calculations on **III** were their experimental X-ray positions and the relative hydrogen atom positions were the MNDO optimized positions; the X-ray positions were also the starting geometries used in the MNDO calculations. Unless otherwise noted, the MNDO structures were optimized with respect to all geometric parameters.

When some of the MNDO results were analyzed, the total electronic energy, E, of the molecules was partitioned as the sum of one-center, E_A, and two-center, E_{AB}, terms such that[17-19]

$$E = \sum_A E_A + \sum\sum_{A<B} E_{AB}$$

E_{AB} has been found to provide a good quantitative measure of the A–B bond strength. A large negative value of E_{AB} indicates bonding between atoms A and B, while a positive value implies antibonding.[18] Such analyses have proved useful in understanding the bonding interactions in a number of the carbons adjacent metallacarboranes.[3i,20]

Results and Discussion

Synthesis and Spectra. The reactions of the THF-solvated disodium compounds, *closo-exo*-5,6-Na(THF)$_2$-1-Na(THF)$_2$-2-(SiMe$_3$)-4-(R)-2,4-$C_2B_4H_4$ (R = SiMe$_3$, Me),[8] with anhydrous $SnCl_2$ in THF in molar ratios of 1:1 at 0 °C produced the carbons apart *closo*-stannacarboranes, 1-Sn-2,4-(SiMe$_3$)$_2$-2,4-$C_2B_4H_4$ (**I**) and 1-Sn-2-(SiMe$_3$)-4-(Me)-2,4-$C_2B_4H_4$ (**II**) as colorless liquids in 86 and 51% yields, respectively (see Scheme 1). The corresponding carbons adjacent isomers have been produced, as off-white solids, in reactions very similar to those shown in Scheme 1. Although no X-ray data could be obtained for **I** and **II**, the structural characterization of the starting carborane dianions,[8] coupled with the spectroscopic similarities of **I** and **II** with their starting carborane dianions and the structurally characterized carbons adjacent *closo*-stannacarboranes 1-Sn-2-(SiMe$_3$)-3-(R)-2,3-$C_2B_4H_4$ (R = SiMe$_3$, Me),[3a,b,h] leave little doubt as to the general validity of the structures shown in Scheme 1. It is of interest to note that the separation of the carbons in the bonding faces of the carborane cages of **I** and **II** gives rise to metallacarboranes with much lower melting points than those of their carbons adjacent analogues. Such a separation should lead to lower molecular polarities and, hence, lower melting points. The MNDO calculated dipole moment of **I** was found to be 2.4 D compared to 3.7 D calculated for the carbons adjacent isomer. The high solubilities of **I** and **II** in nonpolar solvents are also consistent with these molecules having fairly low polarities.

The *closo*-stannacarboranes **I** and **II** are similar to their carbons adjacent isomers[3] in that they react readily with benzene solutions of the Lewis bases, 2,2′-bipyridine, 2,2′-bipyrimidine, (ferrocenylmethyl)-*N*,*N*-dimethylamine, and 2,2′:6′,2″-terpyridine, at room temperature, to form the corresponding donor–acceptor complexes, 1-Sn($C_{10}H_8N_2$)-2,4-(SiMe$_3$)$_2$-2,4-$C_2B_4H_4$ (**III**), 1-Sn($C_8H_6N_4$)-2,4-(SiMe$_3$)$_2$-2,4-$C_2B_4H_4$ (**IV**), 1-Sn($C_8H_6N_4$)-2-(SiMe$_3$)-4-(Me)-2,4-$C_2B_4H_4$ (**V**), 1-Sn[(η^5-C_5H_5)Fe(η^5-$C_5H_4CH_2$(Me)$_2$N)]-2,4-(SiMe$_3$)$_2$-2,4-$C_2B_4H_4$ (**VI**), 1-Sn[(η^5-C_5H_5)Fe(η^5-$C_5H_4CH_2$(Me)$_2$N)]-2-(SiMe$_3$)-4-(Me)-2,4-$C_2B_4H_4$ (**VII**), and 1-Sn($C_{15}H_{11}N_3$)-2,4-(SiMe$_3$)$_2$-2,4-$C_2B_4H_4$ (**VIII**), in 62–95% yields, as shown in Scheme 1. The melting points of **III**, **VI**, and **VII** are 87, 48, and 43 °C, respectively, which are substantially lower than the values of 181.5 ± 0.5, 92 ± 1, and 147 °C found for their respective carbons adjacent analogues.[3-6] The decreases in the melting points of the adducts parallel those found for the uncomplexed

(15) (a) Bursten, B. E.; Fenske, R. F. *J. Chem. Phys.* **1977**, *67*, 3138. (b) Bursten, B. E.; Jensen, R. J.; Fenske, R. F. *J. Chem. Phys.* **1978**, *68*, 3320.
(16) Dewar, M. J. S.; Healy, E. F.; Kuhn, D. R.; Holder, A. J. *Organometallics* **1991**, *10*, 431.
(17) Fisher, H.; Kollmar, H. *Theor. Chim. Acta* **1970**, *16*, 163.
(18) Dewar, M. J. S.; Lo, D. H. *J. Am. Chem. Soc.* **1971**, *93*, 7201.
(19) Olivella, S.; Vilarrusa, J. *J. Heterocycl. Chem.* **1985**, *279*, 359.
(20) (a) Maguire, J. A.; Ford, G. P.; Hosmane, N. S. *Inorg. Chem.* **1988**, *27*, 3354. (b) Maguire, J. A. *Organometallics* **1991**, *10*, 3150.

Table 2. Atomic Coordinates (×10⁴) and Equivalent Isotropic Displacement Coefficients (Å² × 10³)

	x	y	z	U(eq)[a]		x	y	z	U(eq)[a]
				Compound III					
Sn	1310(1)	850(1)	3223(1)	50(1)	C(12)	1223(10)	1350(4)	598(3)	99(3)
Si(1)	2678(2)	2927(1)	3424(1)	54(1)	N(13)	2208(5)	-409(2)	3731(2)	48(1)
Si(2)	2815(3)	786(1)	1222(1)	67(1)	C(14)	2184(8)	-961(3)	3294(3)	60(2)
C(1)	3007(7)	2043(2)	3040(2)	46(2)	C(15)	2371(8)	-1646(3)	3509(3)	68(2)
B(2)	2009(8)	1851(3)	2305(3)	51(2)	C(16)	2537(8)	-1792(3)	4199(3)	62(2)
C(3)	2969(7)	1149(2)	2102(2)	46(2)	C(17)	2575(7)	-1235(3)	4658(2)	52(2)
B(4)	4382(8)	822(3)	2729(3)	50(2)	C(18)	2422(6)	-546(2)	4415(2)	42(2)
B(5)	4449(8)	1436(3)	3355(3)	45(2)	C(19)	2431(6)	81(2)	4871(2)	38(2)
B(6)	4605(8)	1726(3)	2518(3)	52(2)	N(20)	2158(5)	718(2)	4565(2)	43(1)
C(7)	120(8)	2961(3)	3668(3)	71(2)	C(21)	2179(7)	1294(3)	4962(3)	49(2)
C(8)	2970(9)	3636(3)	2771(3)	80(3)	C(22)	2479(7)	1269(3)	5673(3)	51(2)
C(9)	4508(8)	3089(3)	4196(3)	73(2)	C(23)	2745(7)	625(3)	5989(2)	50(2)
C(10)	1739(13)	-113(3)	1222(3)	129(4)	C(24)	2734(6)	25(3)	5587(2)	44(2)
C(11)	5333(11)	712(4)	944(3)	112(3)					
				Compound IV					
Sn	1989(1)	1810(1)	1862(1)	51(1)	C(12)	2495(6)	-624(3)	1208(7)	109(3)
Si(1)	-645(1)	1561(1)	3895(1)	53(1)	N(13)	4151(4)	1991(2)	1120(3)	46(1)
Si(2)	3470(1)	-57(1)	2247(1)	62(1)	C(14)	5020(5)	2333(3)	1812(4)	54(2)
C(1)	862(4)	1320(2)	3460(4)	46(2)	C(15)	6063(5)	2580(3)	1440(5)	66(2)
B(2)	1106(5)	738(3)	2598(5)	50(2)	C(16)	6174(5)	2454(3)	306(5)	80(3)
C(3)	2567(4)	688(2)	2694(4)	46(2)	N(17)	5337(4)	2123(3)	-414(3)	63(2)
B(4)	3254(5)	1277(3)	3511(5)	51(2)	C(18)	4358(4)	1904(2)	25(4)	41(2)
B(5)	2092(5)	1700(3)	3991(5)	46(2)	C(19)	3381(4)	1524(2)	-751(4)	44(2)
B(6)	2040(5)	799(3)	3994(5)	53(2)	N(20)	2499(4)	1226(2)	-245(4)	59(2)
C(7)	-825(5)	2502(3)	3613(6)	78(2)	C(21)	1629(5)	887(3)	-955(6)	77(3)
C(8)	-1947(5)	1103(4)	3066(6)	100(3)	C(22)	1651(6)	843(3)	-2107(6)	78(3)
C(9)	-645(5)	1388(4)	5461(5)	86(3)	C(23)	2591(6)	1171(3)	-2538(5)	74(2)
C(10)	4822(5)	234(3)	1581(5)	78(2)	N(24)	3483(4)	1519(2)	-1873(4)	59(2)
C(11)	4067(7)	-554(3)	3575(6)	100(3)					
				Compound VI					
Sn	3188(1)	4184(1)	4831(1)	44(1)	C(12)	354(14)	4430(2)	656(7)	76(4)
Fe	5911(2)	3196(1)	9550(1)	50(1)	N(13)	4297(8)	4078(1)	7190(4)	40(2)
C(1)	1216(10)	3677(2)	4273(6)	41(3)	C(14)	4564(11)	3722(2)	7487(6)	44(3)
B(2)	1356(12)	3883(2)	3083(7)	43(3)	C(15)	6202(11)	4275(2)	7332(6)	53(3)
C(3)	182(9)	4222(2)	3282(5)	32(2)	C(16)	2717(11)	4242(2)	7892(6)	58(3)
B(4)	-536(12)	4256(2)	4617(7)	39(3)	C(20)	5553(11)	3649(2)	8709(6)	42(3)
B(5)	124(12)	3875(2)	5261(7)	43(3)	C(21)	7674(12)	3585(2)	9002(8)	61(3)
B(6)	-1019(12)	3877(2)	3798(7)	39(3)	C(22)	7934(18)	3540(2)	10260(9)	87(4)
Si(1)	1816(3)	3214(1)	4342(2)	47(1)	C(23)	6030(19)	3580(2)	10738(8)	80(4)
Si(2)	-542(3)	4545(1)	2141(2)	42(1)	C(24)	4584(14)	3652(2)	9807(7)	56(3)
C(7)	680(14)	2998(2)	2970(7)	78(4)	C(25)	3704(17)	2839(3)	9441(21)	118(7)
C(8)	4667(11)	3157(2)	4405(8)	68(3)	C(26)	5089(32)	2784(3)	10424(11)	100(6)
C(9)	772(12)	3011(2)	5673(7)	66(3)	C(27)	6951(23)	2729(2)	10036(15)	101(6)
C(10)	760(12)	4945(2)	2632(7)	70(3)	C(28)	6824(22)	2756(2)	8824(14)	98(6)
C(11)	-3366(12)	4604(3)	2028(9)	101(5)	C(29)	4827(28)	2827(2)	8444(11)	98(5)

[a] Equivalent isotropic U defined as one-third of the trace of the orthogonalized U_{ij} tensor.

stannacarboranes, again demonstrating the effect of cage carbon placement on the physical properties of the resulting metallacarboranes. It is interesting to note that the terpyridine complex (**VIII**) has a melting point of 131 ± 1 °C, which is essentially the same as that of its carbons adjacent isomer (129 ± 1 °C).[3g] Since the structure of **VIII** has not been determined, it is not possible to tell whether this observation has any geometric significance.

All compounds were sufficiently stable so that their formulas could be verified by elemental analyses (see Experimental Section). The structure of **VI** was confirmed by X-ray structural determination; the similarities in the spectra of **VI** and **VII**, as well as their similar methods of synthesis, leave little doubt as to the validity of the formula of **VII**. However, the formulation of **VIII** is based primarily on its solution NMR and IR spectra, as well as the similarity of its synthetic procedure with those of the more extensively characterized donor–acceptor complexes (**III**–**VII**) and its structurally characterized carbons adjacent isomer.[3g] Since there was some question as to whether the terpyridine was functioning as a bidentate or tridentate ligand in the carbons adjacent system and the melting point of **VIII** seems out of line with those found for the other compounds in this study, there is more uncertainty in the geometry of **VIII** than in the other base complexes.

Compounds **I**–**VIII** were characterized by ^{1}H, ^{11}B, ^{13}C, and ^{119}Sn pulse Fourier transform NMR (Table 5), IR (Table 6), and mass spectra (Experimental Section). The ^{1}H and ^{13}C NMR, IR, and mass spectra of the *closo*-stannacarboranes, **I** and **II**, and the corresponding donor–acceptor complexes, **III**–**VIII**, are all consistent with the formulas given in the Experimental Section. The ^{11}B NMR spectra of **I** and **II** are of particular interest. The ^{11}B NMR spectra of **I**–**VIII**, and their carbons adjacent isomers, are similar in that all show resonances in the δ = −5 to −9 ppm region, due to the apical borons, with the basal boron resonances occurring in the δ = 17–25 ppm range. The peaks listed in Table 5, which are all very broad, show peak area patterns of 2:1:1 or 3:1. When the basal boron resonances were resolved (in compounds **I**–**III**), the peak for the unique boron (the boron lying in the pseudomirror plane of the C_2B_4 cage) was shifted slightly upfield from those of the other two basal borons. This is similar to the patterns found in all of the carbons adjacent carboranes and metallacarboranes, with the

Table 3. Bond Lengths (Å) and Bond Angles (deg)

Bond Lengths

Compound III

Sn–Cnt(3)[a]	2.152	Sn–C(1)	2.573 (5)	B(2)–B(6)	1.782 (8)	C(3)–B(4)	1.588 (7)
Sn–B(2)	2.683 (6)	Sn–C(3)	2.640(5)	C(3)–B(6)	1.693 (7)	B(4)–B(5)	1.679 (8)
Sn–B(4)	2.405 (6)	Sn–B(5)	2.393 (5)	B(4)–B(6)	1.762 (8)	B(5)–B(6)	1.738 (8)
Sn–N(13)	2.614 (4)	Sn–N(20)	2.625 (4)	N(13)–C(14)	1.344 (6)	N(13)–C(18)	1.350 (6)
Si(1)–C(1)	1.850 (5)	Si(1)–C(7)	1.861 (6)	C(14)–C(15)	1.358 (8)	C(15)–C(16)	1.366 (8)
Si(1)–C(8)	1.872 (6)	Si(1)–C(9)	1.863 (5)	C(16)–C(17)	1.377 (7)	C(17)–C(18)	1.381 (7)
Si(2)–C(3)	1.839 (5)	Si(2)–C(10)	1.846 (7)	C(18)–C(19)	1.478 (6)	C(19)–N(20)	1.344 (6)
Si(2)–C(11)	1.863 (8)	Si(2)–C(12)	1.863 (6)	C(19)–C(24)	1.393 (6)	N(20)–C(21)	1.332 (6)
C(1)–B(2)	1.555 (7)	C(1)–B(5)	1.583 (7)	C(21)–C(22)	1.378 (7)	C(22)–C(23)	1.364 (7)
C(1)–B(6)	1.686 (7)	B(2)–C(3)	1.548(7)	C(23)–C(24)	1.375 (7)		

Compound IV

Sn–Cnt(4)	2.076	Sn–C(1)	2.552 (5)	B(2)–B(6)	1.800 (8)	C(3)–B(4)	1.609 (7)
Sn–B(2)	2.499 (6)	Sn–C(3)	2.438 (5)	C(3)–B(6)	1.707 (8)	B(4)–B(5)	1.670 (8)
Sn–B(4)	2.439 (6)	Sn–B(5)	2.479 (6)	B(4)–B(6)	1.770 (9)	B(5)–B(6)	1.755 (8)
Sn–N(13)	2.640 (4)	Sn–N(20)	2.832(4)	N(13)–C(14)	1.333 (6)	N(13)–C(18)	1.338 (6)
Si(1)–C(1)	1.844 (5)	Si(1)–C(7)	1.865 (6)	C(14)–C(15)	1.358 (8)	C(15)–C(16)	1.366 (8)
Si(1)–C(8)	1.834 (6)	Si(1)–C(9)	1.857 (6)	C(16)–N(17)	1.320 (7)	N(17)–C(18)	1.315 (7)
Si(2)–C(3)	1.866 (5)	Si(2)–C(10)	1.845 (6)	C(18)–C(19)	1.495 (6)	C(19)–N(20)	1.327 (7)
Si(2)–C(11)	1.865 (7)	Si(2)–C(12)	1.861 (7)	C(19)–N(24)	1.328 (7)	N(20)–C(21)	1.343 (7)
C(1)–B(2)	1.561 (7)	C(1)–B(5)	1.580 (7)	C(21)–C(22)	1.350 (10)	C(22)–C(23)	1.359 (10)
C(1)–B(6)	1.685 (7)	B(2)–C(3)	1.582 (7)	C(23)–N(24)	1.341 (7)		

Compound VI

Sn–Cnt(5)	2.060	Sn–C(1)	2.440 (7)	Fe–Cnt(c2)	1.646	Fe–C(20)	2.031 (7)
Sn–B(2)	2.520 (8)	Sn–C(3)	2.533 (6)	Fe–C(21)	2.039 (8)	Fe–C(22)	2.022 (10)
Sn–B(4)	2.440 (8)	Sn–B(5)	2.415 (8)	Fe–C(23)	2.018 (9)	Fe–C(24)	2.031 (8)
Sn–N(13)	2.723 (5)	C(1)–B(2)	1.569 (11)	Fe–C(25)	2.013 (11)	Fe–C(26)	1.993 (12)
C(1)–B(5)	1.565 (11)	C(1)–B(6)	1.711 (10)	Fe–C(27)	2.028 (11)	Fe–C(28)	2.026 (11)
C(1)–Si(1)	1.874 (7)	B(2)–C(3)	1.566 (10)	Fe–C(29)	2.012 (11)	N(13)–C(14)	1.455 (8)
B(2)–B(6)	1.789 (12)	C(3)–B(4)	1.601 (10)	N(13)–C(15)	1.467 (9)	N(13)–C(16)	1.486 (9)
C(3)–B(6)	1.693 (10)	C(3)–Si(2)	1.847 (6)	C(14)–C(20)	1.500 (9)	C(24)–C(23)	1.387 (13)
B(4)–B(5)	1.710 (11)	B(4)–B(6)	1.772 (11)	C(24)–C(20)	1.418 (11)	C(23)–C(22)	1.393 (17)
B(5)–B(6)	1.753 (11)	Si(1)–C(7)	1.867 (8)	C(22)–C(21)	1.418 (13)	C(21)–C(20)	1.422 (11)
Si(1)–C(8)	1.868 (8)	Si(1)–C(9)	1.861 (8)	C(25)–C(26)	1.393 (25)	C(25)–C(29)	1.376 (26)
Si(2)–C(10)	1.860 (8)	Si(2)–C(11)	1.851 (8)	C(26)–C(27)	1.333 (25)	C(27)–C(28)	1.357 (23)
Si(2)–C(12)	1.855 (8)	Fe–Cnt(c1)	1.637	C(28)–C(29)	1.371 (22)		

Bond Angles

Compound III

Cnt(3)–Sn–N(13)	121.8	Cnt(3)–Sn–N(20)	116.1	C(1)–Si(1)–C(7)	107.3(2)	C(1)–Si(1)–C(8)	109.9(2)
N(13)–Sn–N(20)	61.5(1)	Si(1)–C(1)–B(2)	121.5(3)	C(7)–Si(1)–C(8)	109.2(3)	C(1)–Si(1)–C(9)	111.9(2)
Si(1)–C(1)–B(5)	126.3(3)	B(2)–C(1)–B(5)	111.9(4)	C(7)–Si(1)–C(9)	110.0(2)	C(8)–Si(1)–C(9)	108.6(3)
Si(1)–C(1)–B(6)	132.9(3)	B(2)–C(1)–B(6)	66.6(3)	C(3)–Si(2)–C(10)	108.6(3)	C(3)–Si(2)–C(11)	110.3(3)
B(5)–C(1)–B(6)	64.1(3)	C(1)–B(2)–C(3)	106.5(4)	C(10)–Si(2)–C(11)	108.1(4)	C(3)–Si(2)–C(12)	111.2(3)
C(1)–B(2)–B(6)	60.2(3)	C(3)–B(2)–B(6)	60.6(3)	C(10)–Si(2)–C(12)	108.9(3)	C(11)–Si(2)–C(12)	109.6(3)
Si(2)–C(3)–B(2)	125.3(3)	Si(2)–C(3)–B(4)	122.5(3)	Sn–N(13)–C(14)	118.5(3)	Sn–N(13)–C(18)	122.8(3)
B(2)–C(3)–B(4)	111.6(4)	Si(2)–C(3)–B(6)	130.4(3)	C(14)–N(13)–C(18)	118.0(4)	N(13)–C(14)–C(15)	123.1(5)
B(2)–C(3)–B(6)	66.5(3)	B(4)–C(3)–B(6)	64.9(3)	C(14)–C(15)–C(16)	119.3(5)	C(15)–C(16)–C(17)	118.7(5)
C(3)–B(4)–B(5)	104.8(4)	C(3)–B(4)–B(6)	60.5(3)	C(16)–C(17)–C(18)	119.8(4)	N(13)–C(18)–C(17)	121.0(4)
B(5)–B(4)–B(6)	60.6(3)	C(1)–B(5)–B(4)	104.7(4)	N(13)–C(18)–C(19)	115.7(4)	C(17)–C(18)–C(19)	123.3(4)
C(1)–B(5)–B(6)	60.8(3)	B(4)–B(5)–B(6)	62.1(3)	C(18)–C(19)–N(20)	117.2(4)		
C(1)–B(6)–B(2)	53.2(3)	C(1)–B(6)–C(3)	94.7(4)	C(18)–C(19)–C(24)	122.2(4)	N(20)–C(19)–C(24)	120.6(4)
B(2)–B(6)–C(3)	52.8(3)	C(1)–B(6)–B(4)	97.0(4)	Sn–N(20)–C(19)	122.0(3)	Sn–N(20)–C(21)	119.3(3)
B(2)–B(6)–B(4)	94.1(4)	C(3)–B(6)–B(4)	54.7(3)	C(19)–N(20)–C(21)	118.6(4)	N(20)–C(21)–C(22)	123.3(4)
C(1)–B(6)–B(5)	55.0(3)	B(2)–B(6)–B(5)	95.2(4)	C(21)–C(22)–C(23)	118.7(5)	C(22)–C(23)–C(24)	118.9(4)
C(3)–B(6)–B(5)	98.0(4)	B(4)–B(6)–B(5)	57.4(3)	C(19)–C(24)–C(23)	120.0(4)		

Compound IV

Cnt(4)–Sn–N(13)	116.1	Cnt(4)–Sn–N(20)	116.7	C(7)–Si(1)–C(8)	109.3(3)	C(1)–Si(1)–C(9)	110.2(2)
N(13)–Sn–N(20)	58.6(1)	Si(1)–C(1)–B(2)	126.7(3)	C(7)–Si(1)–C(9)	109.7(3)	C(8)–Si(1)–C(9)	109.0(3)
Si(1)–C(1)–B(5)	120.7(3)	B(2)–C(1)–B(5)	112.5(4)	C(3)–Si(2)–C(10)	111.1(2)	C(3)–Si(2)–C(11)	108.0(3)
Si(1)–C(1)–B(6)	135.4(4)	B(2)–C(1)–B(6)	67.2(3)	C(10)–Si(2)–C(11)	107.6(3)	C(3)–Si(2)–C(12)	111.6(3)
B(5)–C(1)–B(6)	64.9(3)	C(1)–B(2)–C(3)	104.9(4)	C(10)–Si(2)–C(12)	109.0(3)	C(11)–Si(2)–C(12)	109.6(3)
C(1)–B(2)–B(6)	59.7(3)	C(3)–B(2)–B(6)	60.2(3)	Sn–N(13)–C(14)	117.3(3)	Sn–N(13)–C(15)	145.0(2)
Si(2)–C(3)–B(2)	126.3(3)	Si(2)–C(3)–B(4)	119.9(3)	Sn–N(13)–C(18)	124.8(3)	C(14)–N(13)–C(18)	116.2(4)
B(2)–C(3)–B(4)	112.3(4)	Si(2)–C(3)–B(6)	126.9(3)	N(13)–C(14)–C(15)	122.6(5)	C(14)–C(15)–C(16)	115.8(5)
B(2)–C(3)–B(6)	66.3(3)	B(4)–C(3)–B(6)	64.5(3)	C(15)–C(16)–N(17)	123.9(6)	C(16)–N(17)–C(18)	115.9(5)
C(3)–B(4)–B(5)	103.8(4)	C(3)–B(4)–B(6)	60.5(3)	N(13)–C(18)–N(17)	125.6(4)	N(13)–C(18)–C(19)	116.2(4)
B(5)–B(4)–B(6)	61.3(3)	C(1)–B(5)–B(4)	106.1(4)	C(14)–C(18)–C(19)	148.0(4)	C(16)–C(18)–C(19)	150.3(4)
C(1)–B(5)–B(6)	60.4(3)	B(4)–B(5)–B(6)	62.2(3)	N(17)–C(18)–C(19)	118.2(4)	C(18)–C(19)–N(20)	116.5(4)
C(1)–B(6)–B(2)	53.1(3)	C(1)–B(6)–C(3)	94.6(4)	C(18)–C(19)–C(21)	148.8(4)	C(18)–C(19)–C(23)	149.5(4)
B(2)–B(6)–C(3)	53.5(3)	C(1)–B(6)–B(4)	97.5(4)	C(18)–C(19)–N(24)	116.8(4)	N(20)–C(19)–N(24)	126.7(4)
B(2)–B(6)–B(4)	95.8(4)	C(3)–B(6)–B(4)	55.1(3)	Sn–N(20)–C(19)	116.7(3)	Sn–N(20)–C(21)	121.8(4)
C(1)–B(6)–B(5)	54.6(3)	B(2)–B(6)–B(5)	94.5(4)	C(19)–N(20)–C(21)	115.7(5)	Sn–N(20)–C(22)	145.8(2)
C(3)–B(6)–B(5)	96.3(4)	B(4)–B(6)–B(5)	56.5(3)	N(20)–C(21)–C(22)	122.5(6)	C(21)–C(22)–C(23)	117.1(6)
C(1)–Si(1)–C(7)	106.1(3)	C(1)–Si(1)–C(8)	112.6(3)	C(22)–C(23)–N(24)	123.1(5)	C(19)–N(24)–C(23)	114.9(5)

Table 3 (Continued)

				Compound VI			
Cnt(5)–Sn–N(13)	119.3	B(2)–C(1)–B(5)	113.2(6)	C(7)–Si(1)–C(8)	108.4(4)	C(1)–Si(1)–C(9)	111.7(3)
B(2)–C(1)–B(6)	66.0(5)	B(5)–C(1)–B(6)	64.5(5)	C(7)–Si(1)–C(9)	108.3(4)	C(8)–Si(1)–C(9)	109.5(4)
B(2)–C(1)–Si(1)	121.3(5)	B(5)–C(1)–Si(1)	124.3(5)	C(3)–Si(2)–C(10)	107.1(3)	C(3)–Si(2)–C(11)	110.0(4)
B(6)–C(1)–Si(1)	129.5(5)	C(1)–B(2)–C(3)	105.5(6)	C(10)–Si(2)–C(11)	110.2(4)	C(3)–Si(2)–C(12)	111.6(3)
C(1)–B(2)–B(6)	60.8(4)	C(3)–B(2)–B(6)	60.2(4)	C(10)–Si(2)–C(12)	108.0(4)	C(11)–Si(2)–C(12)	109.9(4)
B(2)–C(3)–B(4)	112.3(5)	B(2)–C(3)–B(6)	66.5(5)	Cnt(c1)–Fe–Cnt(c2)[b]	178.5	Sn–N(13)–C(14)	113.0(4)
B(4)–C(3)–B(6)	65.0(4)	B(2)–C(3)–Si(2)	126.8(5)	Sn–N(13)–C(15)	101.0(4)	Sn–N(13)–C(16)	107.2(4)
B(4)–C(3)–Si(2)	120.7(5)	B(6)–C(3)–Si(2)	133.7(4)	C(14)–N(13)–C(15)	113.8(5)	C(14)–N(13)–C(16)	112.3(5)
C(3)–B(4)–B(5)	103.8(6)	C(3)–B(4)–B(6)	60.0(4)	C(15)–N(13)–C(16)	108.7(5)	N(13)–C(14)–C(20)	115.5(5)
B(5)–B(4)–B(6)	60.4(4)	C(1)–B(5)–B(4)	104.8(6)	Fe–C(20)–C(14)	128.3(5)	Fe–C(20)–C(21)	69.8(4)
C(1)–B(5)–B(6)	61.8(5)	B(4)–B(5)–B(6)	61.5(5)	Fe–C(20)–C(24)	69.5(4)	C(14)–C(20)–C(24)	126.8(7)
C(1)–B(6)–B(2)	53.2(4)	C(1)–B(6)–C(3)	94.3(5)	C(14)–C(20)–C(21)	126.6(7)	C(24)–C(20)–C(21)	106.5(6)
B(2)–B(6)–C(3)	53.4(4)	C(1)–B(6)–B(4)	96.4(5)	C(22)–C(21)–C(20)	107.5(8)	C(23)–C(22)–C(21)	108.5(9)
B(2)–B(6)–B(4)	95.2(5)	C(3)–B(6)–B(4)	55.0(4)	C(24)–C(23)–C(22)	108.2(8)	C(23)–C(24)–C(20)	109.2(8)
C(1)–B(6)–B(5)	53.7(4)	B(2)–B(6)–B(5)	95.2(5)	C(26)–C(25)–C(29)	106.4(12)	C(25)–C(26)–C(27)	108.9(14)
C(3)–B(6)–B(5)	98.3(5)	B(4)–B(6)–B(5)	58.0(4)	C(26)–C(27)–C(28)	108.5(13)	C(27)–C(28)–C(29)	108.6(14)
C(1)–Si(1)–C(7)	110.0(3)	C(1)–Si(1)–C(8)	108.9(3)	C(25)–C(29)–C(28)	107.5(13)		

[a] Cnt(3), Cnt(4), and Cnt(5): the centroid of the C2B3 ring in structures **III**, **IV**, and **V**, respectively. [b] Cnt(c1) and Cnt(c2): the centroid of the Cp ring of ferrocene.

Table 4. Mean Deviations (Å) and Dihedral Angles (deg) of the Least-Squares Planes

plane	III	IV	VI
	Mean Deviations		
plane 1 [C_2B_3 ring]	0.027	0.025	0.021
plane 2 [$C_{10}N_2$ Bpy ring]	0.026		
plane 3 [C_8N_4 Bpmd ring]		0.066	
plane 4 [$C_5N(1)$ pyri ring]	0.007		
plane 5 [$C_5N(2)$ pyri ring]	0.002		
plane 6 [$C_4N_2(1,2)$ pyraz ring]		0.002	
plane 7 [$C_4N_2(3,4)$ pyraz ring]		0.003	
plane 8 [(C_5CNMe_2)Fe ring]			0.007
plane 9 [(C_5)Fe ring]			0.007
	Dihedral Angles		
1 and 2	33.3		
1 and 3		48.7	
1 and 4	35.0		
1 and 5	31.8		
1 and 6		44.0	
1 and 7		53.4	
1 and 8			55.2
1 and 9			55.2
4 and 5	3.4		
6 and 7		9.5	
8 and 9			2.0

exception of the ferrocene amine–stannacarborane complexes.[3f,9] The only other exceptions to the 2:1:1 peak area patterns were found in the more ionic group 1 carborane precursors of **I** and **II**, in which ^{11}B NMR spectra show three well resolved resonances with peak area ratios of 1:2:1.[8] This 1:2:1 pattern was explained on the basis that, because of its position between the more electronegative cage carbons, the unique boron would be more deshielded than the other basal borons, which would result in its ^{11}B NMR resonance being shifted downfield from the other two basal borons. The change from a 1:2:1 to a 2:1:1 ^{11}B NMR pattern on forming **I–VIII** is clearly the result of tin bonding; since a similar rearrangement was also found on nickel bonding,[8a] the 2:1:1 pattern can probably be taken as diagnostic of metal–carborane covalent bonding in the carbons apart system. These changes in peak area patterns cannot be traced to the change in any one particular resonance position. Metal complexation causes downfield shifts of all the boron resonances; for the basal borons, the resonances of the two equivalent borons undergo slightly greater downfield shifts than do those of the unique borons. On the other hand, the changes in the chemical shifts of the apical boron resonances in **I–VII** are more easily rationalized, in that they follow the same pattern as found in the carbons adjacent system, that is, a large downfield shift when the carborane initially bonds to the tin (δ for the apical boron of **I** is −9.03 ppm, compared to a value of −45.86 ppm for its disodium salt),[8b] followed by a more modest shift back upfield when the tin coordinates to a Lewis base. These shifts have been explained on the basis of the apical boron competing with the capping metal for electron density: initial bonding by the metal will draw electron density away from the apical boron, causing a large downfield shift; coordination of the metal by a Lewis base would tend to restore some electron density to the apical boron, resulting in a shift back upfield.[8a,20] Although the shifts found for compounds **I–VII** are not as large as those found in the corresponding carbons adjacent isomers, they are in line with the expected change in electron density on the apical boron. The unshifted apical boron resonance in **VIII**, compared to its precursor, **I**, could indicate that a very weak base–stannacarborane complex exists between **I** and 2,2′:6′,2″-terpyridine. Since the C_2B_3 ring acts as the link through which electron density is transferred from the apical boron to the metal, and back, the electron density on these atoms should be less effected by metal–carborane bonding than that on the apical boron and undergo smaller chemical shift changes. Because considerations other than gross electron density have been shown to be important in determining the ^{11}B NMR chemical shifts in heterocarboranes,[21] it is difficult to interpret the chemical shifts shown in Table 5 directly in terms of bonding strengths or complex geometries.

By far the most interesting spectroscopic data are the chemical shifts found in the ^{119}Sn NMR spectra of the compounds (see Table 5). The ^{119}Sn resonances of **I** and **II** appear at δ = −533.06 and −535.27 ppm, respectively, compared to δ's of −206 and −171 ppm for their respective carbons adjacent isomers.[22] These upfield shifts are the largest shifts reported for any of the *closo-* or *commo*-stannacarboranes in the C_2B_4 systems.[22,23] It is surprising that the separation of the carbon atoms in the C_2B_3 pentagonal face should result in as large an increase in the shielding of the apical tin atom as is found in **I** and **II**. Table 5 shows that, on coordination with a Lewis base, the ^{119}Sn NMR resonances shift upfield by 5 ppm (**VI**) to 79

(21) (a) Hermánek, S.; Hnyk, D.; Havlas, Z. *J. Chem. Soc., Chem. Commun.* **1989**, 1859. (b) Bühl, M.; Schleyer, P. v. R.; Havlas, Z.; Hnyk, D.; Hermánek *Inorg. Chem.* **1991**, *30*, 3107.

(22) Hosmane, N. S.; Sirmokadam, N. N.; Herber, R. H. *Organometallics* **1984**, *3*, 1665.

(23) Jia, L.; Zhang, H.; Hosmane, N. S. *Organometallics* **1992**, *11*, 2957.

Table 5. FT NMR Spectral Data[a]

compd	δ splitting, assignt [$^1J(^{11}B-^1H)$ or $^1J(^{13}C-^1H)$, Hz]	rel areas
	200.13-MHz ^1H NMR Data[b]	
I	4.83, q (br), overlapping, basal H_t[$^1J(^1H-^{11}B)$ = 143]; 4.44, q (br), overlapping, basal H_t[$^1J(^1H-^{11}B)$ = 146]; 3.51, q (br), apical H_t[$^1J(^1H-^{11}B)$ = 169]; 0.27, s, $SiMe_3$	2:1:1:18
II	4.79, q (br), overlapping, basal H_t[$^1J(^1H-^{11}B)$ = 140]; 4.62, q (br), overlapping, basal H_t[$^1J(^1H-^{11}B)$ = 145]; 4.39, q (br), overlapping, basal H_t[$^1J(^1H-^{11}B)$ = 151]; 3.43, q (br), apical H_t [$^1J(^1H-^{11}B)$ = 164]; 2.27, s (br), C–Me; 0.27, s, $SiMe_3$	1:1:1:1:3:9
III	8.45, d, bpy ring, [$J(^1H-^1H)$ = 5.21]; 8.41, d, bpy ring [$J(^1H-^1H)$ = 7.9]; 7.14, t, bpy ring [$^3J(^1H-^1H)$ = 7.92]; 6.63, t, bpy ring [$J(^1H-^1H)$ = 5.25]; 4.77, q (br), overlapping, basal H_t[$^1J(^1H-^{11}B)$ = 107]; 4.63, q (br), overlapping, basal H_t[$^1J(^1H-^{11}B)$ = unresolved]; 2.95, q (br), apical H_t[$^1J(^1H-^{11}B)$ = 165]; 0.08, s, $SiMe_3$	2:2:2:2:2:1:1:18
IV	8.42, d (br), bpmd ring [$J(^1H-^1H)$ = 4.86]; 6.40, t (br), bpmd ring [$J(^1H-^1H)$ = 4.86]; 4.91, q (br), overlapping, basal H_t[$^1J(^1H-^{11}B)$ = unresolved]; 2.53, q (br), apical H_t[$^1J(^1H-^{11}B)$ = 168]; 0.21, s, $SiMe_3$	4:2:3:1:18
V	8.39, d (br), bpmd ring [$J(^1H-^1H)$ = 4.89]; 6.36, t (br), bpmd ring [$J(^1H-^1H)$ = 4.90]; 4.87, q (br), overlapping, basal H_t[$^1J(^1H-^{11}B)$ = unresolved]; 2.46, q (br), apical H_t[$^1J(^1H-^{11}B)$ = 164]; 1.68, s (br), C–Me; 0.30, s, $SiMe_3$	4:2:3:1:3:9
VI	4.92, q (br), overlapping, basal H_t[$^1J(^1H-^{11}B)$ = unresolved]; 4.00, s, C_5H_4 ring; 3.94, s, C_5H_5 ring; 3.24, q (br), apical H_t[$^1J(^1H-^{11}B)$ = 165]; 3.14, s, CH_2; 2.01, s, $N(CH_3)_2$; 0.168, s, $SiMe_3$	3:4:5:1:2:6:18
VII	4.71, q (br), basal H_t[$^1J(^1H-^{11}B)$ = unresolved]; 4.08, s, C_5H_4 ring; 3.98, s, C_5H_5 ring; 3.35, q (br), apical H_t[$^1J(^1H-^{11}B)$ = 158]; 3.23, s, CH_2; 2.66, s (br), C–Me; 2.04, s, $N(CH_3)_2$; 0.42, s, $SiMe_3$	3:4:5:1:2:3:6:9
VIII	8.71, d, terpy ring [$J(^1H-^1H)$ = 7.23]; 8.60, d, 2H, terpy ring [$J(^1H-^1H)$ = 8.0]; 8.54, d, overlapping, terpy ring [$J(^1H-^1H)$ = 7.92]; 7.44, t, terpy ring [$J(^1H-^1H)$ = 8.01]; 7.39, t, terpy ring [$J(^1H-^1H)$ = 8.21]; 6.79, t, terpy ring [$J(^1H-^1H)$ = 7.21]; 4.82, q (br), basal H_t[$^1J(^1H-^{11}B)$ = 125]; 2.98, q, apical H_t[$^1J(^1H-^{11}B)$ = 162]; 0.25, s, $SiMe_3$	2:2:2:1:2:2:3:1:18
	64.21-MHz ^{11}B NMR Data[c]	
I	21.35, d, basal BH (143); 19.45, d, basal BH (146); –9.03, d, apical BH (169)	2:1:1
II	20.57, d, basal BH (139.9); 18.82, d, basal BH (145); 17.44, d, basal BH (151.4); –7.13, apical BH (163.8)	1:1:1:1
III	21.25, d (br), basal BH (106.7); 19.97, d (br), basal BH (115); –11.52, d, apical BH (166.3)	2:1:1
IV	20.88, v br, ill-defined peak, basal BH (unresolved); –13.10, d, apical BH (168)	3:1
V	19.12, v br, ill-defined peak, basal BH (unresolved); –13.36, d, apical BH (163.5)	3:1
VI	20.84, br, ill-defined peak, basal BH (unresolved); –10.81, d, apical BH (165)	3:1
VII	18.20, v br, ill-defined peak, basal BH (unresolved); –9.87, d, apical BH (157.5)	3:1
VIII	21.46, d (br), basal BH (124.4); –9.04, d, apical BH (162.3)	3:1
	50.32-MHz ^{13}C NMR Data[b,d]	
I	114.04, s (br), cage C (SiCB); 1.18, q, $SiMe_3$ (119)	1:3
II	118.6, s (br), cage C (SiCB); 110.8, s (br), cage C (CCB); 21.6, q (br), cage Me (128.9); 1.18, q (br), $SiMe_3$(119.3)	1:1:1:3
III	156.30, s, bpy ring; 149.15, d, bpy ring (176); 136.54, d, bpy ring (162); 123.62, d, bpy ring (163); 121.03, d, bpy ring(160); 112.94, s (br), cage C (SiCB); 0.37, q, $SiMe_3$ (119)	1:1:1:1:1:1:3
IV	163.32, s, bpmd ring; 157.33, d, bpmd ring (183); 121.15, d, bpmd ring (170); 111.96, s (br), cage C (SiCB); 0.57, q, $SiMe_3$ (119)	1:2:1:1:3
V	162.40, s, bpmd ring; 157.16, d, bpmd ring (183); 121.34, d, bpmd ring (170); 115.50, s (br), cage C (SiCB); 107.30, s (br), cage C(CCB); 19.44, q (br), cage Me (127); 0.64, q, $SiMe_3$ (118.9)	2:4:2:1:1:1:3
VI	113.12, s (br), cage C (SiCB); 83.28, s, C_5H_4 ring; 70.46, d, C_5H_4 ring (169); 68.87, d, C_5H_5 ring (175); 68.62, d, C_5H_4 ring (175); 59.08, t, NCH_2 (133); 44.60, q, NCH_3 (133); 0.57, q, $SiMe_3$ (119)	2:1:2:5:2:1:2:6
VII	116.4, s (br), cage C (SiCB); 109.0, s (br), cage C (CCB); 82.82, s, C_5H_4 ring; 70.56, d, C_5H_4 ring (174); 68.80, d, C_5H_5 ring (175); 68.34, d, C_5H_4 ring (175); 59.15, t, NCH_2 (135); 44.71, q, NCH_3 (133); 23.68, q (br), cage Me (126); 1.25, q, $SiMe_3$ (119)	1:1:1:2:5:2:1:2:1:3
VIII	156.75, s, terpy ring; 155.80, s, terpy ring; 149.36, d, terpy ring (178.2); 137.82, d, terpy ring (162.6); 136.37, d, terpy ring (162.8); 123.56, d, terpy ring (164); 121.41, d, terpy ring (164.7); 121.02, d, terpy ring (164.3); 114.79, s (br), cage C(SiCB); 1.51, q, $SiMe_3$ (118.1)	2:2:2:1:2:2:2:2:2:6
	74.63-MHz ^{119}Sn NMR Data[e]	
I	–533.06, s (br), cage Sn	
II	–535.27, s (br), cage Sn	
III	–553.66, s (br), cage Sn bpy	
IV	–587.87, s (br), cage Sn bpmd	
V	–614.24, s (br), cage Sn bpmd	
VI	–537.64, s (br), cage Sn ferrocene amine	
VII	–553.04, s (br), cage Sn ferrocene amine	
VIII	–549.41, s (br), cage Sn terpy	

[a] C_6D_6 was used as solvent and an internal standard of δ = 7.15 ppm (in the ^1H NMR spectra) and δ = 128.0 ppm (in the ^{13}C NMR spectra), with a positive sign indicating a downfield shift. Legend: s = singlet, d = doublet, t = triplet, q = quartet, v = very, br = broad. [b] Shifts relative to external Me_4Si. [c] Shifts relative to external $BF_3{\cdot}OEt_2$. [d] Since relaxation of carbon without H is much slower than that of a CH unit, the relative areas of the substituted carbons of the cage, ferrocene amine, bipyridine, bipyrimidine, and terpyridine units could not be measured accurately. [e] Shifts relative to external Me_4Sn.

Table 6. Infrared Absorptions (cm^{-1}; C_6D_6 vs C_6D_6)[a]

compd	absorption
I	2945 (vs), 2890 (ms) [ν(C—H)], 2560 (vs), 2544 (vs) [ν(B—H)], 1440 (ws), 1400 (ws) [$\delta(CH)_{asym}$], 1340 (wbr), 1260 (ms), 1249 (vs) [$\delta(CH)_{sym}$], 1145 (ms), 1140 (ms), 1070 (wbr), 1020 (ms), 960 (ws), 825 (vvs) [ρ(CH)], 760 (wbr), 680 (ws), 615 (ss), 425(ss)
II	2920 (sh), 2880 (sh), 2865 (vs) [ν(C—H)], 2505 (vs) [ν(B—H)], 2260 (ms), 1340 (sh), 1320 (sh), 1300 (vs), 1240 (vs) [$\delta(CH)_{sym}$], 1180 (ms), 1130 (vs), 1005 (wbr), 960 (wbr), 830 (vs) [ρ(CH)], 750 (vs), 680 (ms), 615 (ms), 480 (vsbr)
III	3080 (ss), 3058 (ss), 3019 (ss) [ν(C—N)], 2960 (vss), 2900 (ms) [ν(C—H)], 2560 (vs), 2410 (sh) [ν(B—H)], 2310 (wbr), 2180 (wbr), 1990 (ws), 1960 (ws), 1925 (wbr), 1885 (wbr), 1860 (wbr), 1795 (wbr), 1710 (wbr), 1655 (wbr), 1586 (vvs), 1565 (vss), 1465 (sbr), 1440 (msh), 1425 (msh) [$\delta(CH)_{asym}$], 1315 (ms), 1260 (ss), 1250 (vvs) [$\delta(CH)_{sym}$], 1150 (vss), 1095 (vss), 1070 (ms), 1045 (vss), 998 (ss), 965 (ms), 921 (ss), 884 (ss), 835 (vvs) [ρ(CH)], 760 (vvs), 690 (ms), 655 (ss), 620 (vss), 600 (ws), 550 (wbr), 435 (ss), 400 (ss)
IV	3040 (ms) [ν(C—N)], 2950 (ss), 2890 (ms) [ν(C—H)], 2530 (vs br) [ν(B—H)], 2245 (ms) [ν(C=N)], 1550 (sbr), 1400 (sbr) [$\delta(CH)_{asym}$], 1320 (wbr), 1245 (ss) [$\delta(CH)_{sym}$], 1050 (mbr), 970 (wbr), 918 (ms), 880 (ms), 830 (wsbr), 800 (msh) [ρ(CH)], 765 (ms), 750 (msh), 670 (ms), 630 (mbr), 490 (vsbr), 430 (ms)
V	3037 (ms) [ν(C—N)], 2962 (ss), 2902 (ms) [ν(C—H)], 2558 (vsbr), 2491 (sbr) [ν(B—H)], 2276 (ms) [ν(C=N)], 1562 (sbr), 1408 (sbr) [$\delta(CH)_{asym}$], 1261 (ss) [$\delta(CH)_{sym}$], 1095 (vvsbr), 1016 (vvsbr), 816 (sh), 800 (sh) [ρ(CH)], 755 (ms), 684 (ms), 630 (mbr), 522 (ws), 490 (vsbr), 484 (ms)
VI	3098 (ss) [ν(C—N)], 2940 (vvs), 2884 (ss), 2850 (ms), 2803 (ss), 2760 (vss) [ν(C—H)], 2545 (vvs), 2530 (vvs) [ν(B—H)], 2260 (ss), 1550 (wbr), 1450 (mbr), 1400 (ms) [$\delta(C—H)_{asym}$], 1390 (ws), 1350 (ws), 1280 (vsbr) [$\delta(CH)_{sym}$], 1190 (vsbr), 1101 (ss), 1030 (vsbr), 1000 (ms), 960 (wbr), 915 (ss), 875 (ss), 825 (vsbr) [ρ(CH)], 765 (ms), 750 (ss), 680 (ms), 620 (ss), 490 (ss)
VII	3088 (ss), 3071 (ss) [ν(C—N)], 3037 (ms), 2967 (ms), 2939 (sh), 2905 (sh), 2886 (ws), 2854 (vss), 2813 (ssh), 2765 (msh) [ν(C—H)], 2532 (vsbr) [ν(B—H)], 1959 (ss), 1815 (vss), 1508 (ws), 1482 (vsbr), 1411 (mbr) [$\delta(C—H)_{asym}$], 1348 (ms), 1261 (vsbr), 1231 (msh) [$\delta(CH)_{sym}$], 1170 (ss), 1136 (ms), 1105 (vss), 1036 (vsbr), 1001 (vssh), 927 (ws), 820 (vvsbr) [ρ(CH)], 755 (ms), 688 (vsbr), 663 (sh), 630 (ws), 616 (sh), 553 (wsh), 512 (vssh), 499 (vssh), 485 (vss), 458 (wsh)
VIII	3072 (ws), 3049 (ws), 2955 (ms), 2857 (ms) [δ(C—H)], 2548 (mbr) [ν(B—H)], 2387 (ms), 2278 (vs), 1975 (ms), 1902 (ws), 1861 (ws), 1798 (ws), 1680 (ws), 1617 (ms), 1581 (ws), 1563 (ms), 1550 (ws), 1452 (ss), 1422 (ms) [$\delta(CH)_{asym}$], 1391 (ms), 1328 (ss), 1261 (ms), 1250 (ms) [$\delta(CH)_{sym}$], 1162 (ms), 1103 (ws), 1039 (ws), 1014 (ms), 944 (ws), 929 (wbr), 841 (mbr), 814 (vvsbr) [ρ(CH)], 771 (ms), 680 (ms) [ν(Si—C)], 664 (ws), 656 (ws), 630 (ws), 518 (mbr), 512 (vsbr), 420 (ws), 365 (ws)

[a] Legend: v = very, s = strong or sharp, m = medium, w = weak, sh= shoulder, and br = broad.

Scheme 1

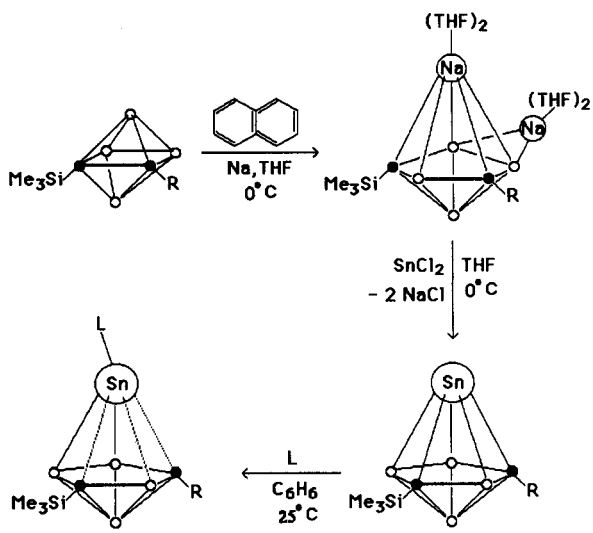

○ = BH ● = C R = $SiMe_3$, Me

L = $C_{10}H_8N_2$, $C_8H_6N_4$, $(\eta^5\text{-}C_5H_5)Fe(\eta^5\text{-}C_5H_4CH_2(Me)_2N)$, $C_{15}H_{11}N_3$

ppm (V); this is in the opposite direction from the changes found in the ^{119}Sn chemical shifts of the corresponding carbons adjacent stannacarboranes, where downfield shifts of 30–150 ppm were found on complexation with the same Lewis bases used in the present study.[3,22] The ^{119}Sn NMR chemical shifts of several other Sn(II)–π complexes have been reported, including $(C_5H_5)_2Sn$ (δ = −2199),[24] $(C_5H_4Me)_2Sn$ (δ = −2171),[25] $(Me_5C_5)_2Sn$ (δ = −2129),[26] $[Me_5C_5Sn]^+$ (δ = −2247),[26] and $Me_2C_2B_9H_9Sn$ (δ = −379).[26] The large upfield shifts found for these complexes cannot be correlated with total tin electron density. The ^{119}Sn NMR chemical shifts have been shown to depend primarily on the value of the "paramagnetic" component of the shielding constant, as defined by Ramsey.[24,27] Wrackmeyer has argued that circulation of charge from the trigonal plane to the underoccupied Sn(5pπ) orbital of $Sn[N(SiMe_3)_2]_2$ effectively deshields the tin, producing a large downfield resonance for this compound at δ = 775 ppm.[24] On the other hand, the large upfield shifts found in the stannocenes have been explained on the basis of the large energy differences that exist between the highest occupied tin containing molecular orbitals [the HOMO's] and the lowest energy unoccupied orbitals having a sizable character of an underutilized Sn(5p) orbital [the LUMO(p)'s], preventing efficient paramagnetic charge circulation in these molecules.[24] Preliminary molecular orbital results for several base–stannacarborane complexes are consistent with such arguments.[28] However, the lack of an extended quantum mechanical analysis of the ^{119}Sn nuclear shielding constants makes it impossible to assess the relative importance of the different factors influencing the chemical

(24) Wrackmeyer, B. *Ann. Rep. NMR Spectrosc.* **1985**, *16*, 73 and references therein.
(25) Bonny, A.; McMaster, A. D.; Stobart, S. R. *Inorg. Chem.* **1978**, *17*, 935.
(26) Jutzi, P. *J. Organomet. Chem.* **1990**, *400*, 1 and references therein.
(27) Ramsey, N. F. *Phys. Rev.* **1950**, *78*, 699.

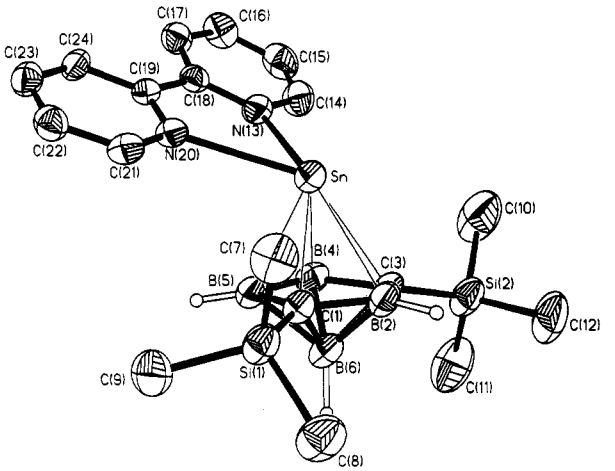

Figure 1. Perspective view of 1-Sn($C_{10}H_8N_2$)-2,4-($SiMe_3$)$_2$-2,4-$C_2B_4H_4$ (**III**) showing the atom numbering scheme with thermal ellipsoids drawn at the 40% probability level. The $SiMe_3$ and the 2,2′-bipyridine H's are omitted for clarity.

shift of the tin. It has been argued that the higher upfield ^{119}Sn chemical shift found in stannocene compared to $Me_2C_2B_9H_9Sn$ might indicate that the dicarbollide ion is less strongly coordinating and less electron donating than the cyclopentadienide ligand.[26] The fact that the ^{119}Sn chemical shifts change in opposite directions when the carbons apart and carbons adjacent stannacarboranes coordinate with the same Lewis bases[3f,g,22] indicates that the relationship between the chemical shift of the tin and its chemical environment is complex and that any conclusions regarding ligand coordinating ability and electron donating ability based solely on ^{119}Sn chemical shift data are, at best, tentative. Although tin-119 chemical shift data can potentially serve as a sensitive probe of tin–ligand π bonding interactions, a great deal more experimental and theoretical work needs to be done before reliable and generally applicable interpretations of ^{119}Sn chemical shifts are possible for these systems.

The IR spectra of compounds **I–VIII** (see Table 6) all show absorptions around 2600 cm^{-1} due to B—H stretching vibrations. The infrared absorptions due to C—N and C=N stretching modes in 2,2′-bipyridine, 2,2′-bipyrimidine, ferrocene amine, and 2,2′:6′,2″-terpyridine are also present near 3080, 3058, 3019, and 2245 cm^{-1}, respectively. These observations are all consistent with the formulas proposed for **I–VIII** but offer little insight into the various bonding interactions that contribute to the structures of these compounds; the IR spectral data shown in Table 6 are listed for purposes of qualitative analyses.

Crystal Structures of 1-Sn($C_{10}H_8N_2$)-2,4-($SiMe_3$)$_2$-2,4-$C_2B_4H_4$ (III), 1-Sn-($C_8H_6N_4$)-2,4-($SiMe_3$)$_2$-2,4-$C_2B_4H_4$ (IV), and 1-Sn[(η^5-C_5H_5)Fe(η^5-$C_5H_4CH_2(Me)_2N$)]-2,4-($SiMe_3$)$_2$-2,4-$C_2B_4H_4$ (VI) and Molecular Orbital Analysis. The solid state structures of **III**, **IV**, and **VI** have been determined by single crystal X-ray diffraction. Figures 1–3 show the structures of these complexes; Table 3 lists some important bond distances and bond angles, and Table 4 gives the mean deviations between some important planes of atoms in the molecules as well as the dihedral angles between those planes.

(28) Fenske–Hall calculations yielded the following Sn $5p_x$, $5p_y$, $5p_z$ orbital populations and HOMO–LUMO(p) gaps (in eV): for $(C_5H_5)_2Sn$, 0.787, 0.843, 0.299, and 22.95; for **III**, 0.870, 0.560, 0.874, and 8.86; for 1-($C_{10}H_8N_2$)Sn-2,3-($SiMe_3$)$_2$-2,3-$C_2B_4H_4$, 0.867, 0.654, 0.895, and 8.08, respectively.

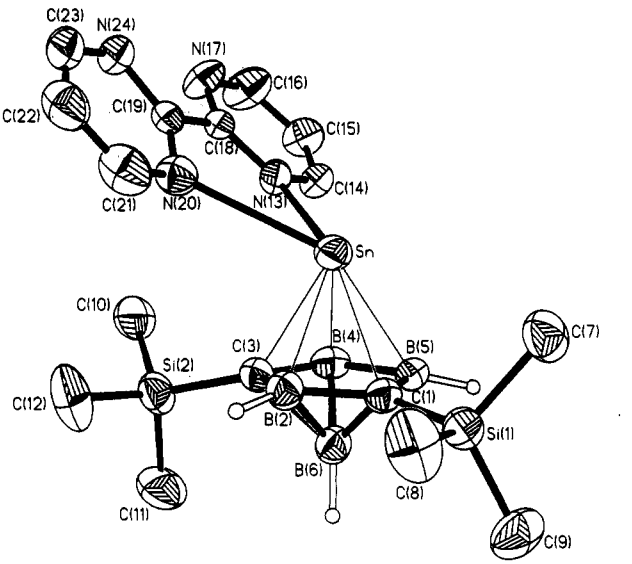

Figure 2. Perspective view of 1-Sn($C_8H_6N_4$)-2,4-($SiMe_3$)$_2$-2,4-$C_2B_4H_4$ (**IV**) showing the atom numbering scheme with thermal ellipsoids drawn at the 40% probability level. The $SiMe_3$ and the 2,2′-bipyrimidine H's are omitted for clarity.

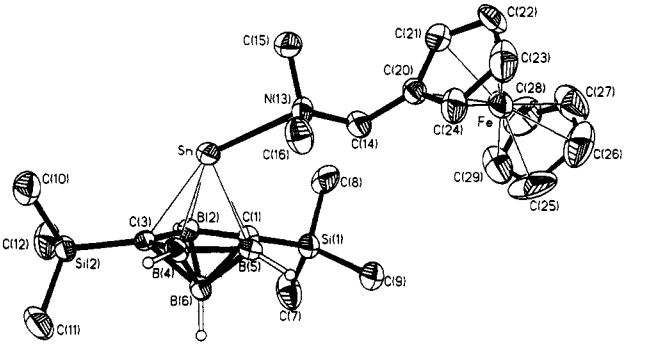

Figure 3. Perspective view of 1-Sn[(η^5-C_5H_5)Fe(η^5-$C_5H_4CH_2$-$(Me)_2N$)]-2,4-($SiMe_3$)$_2$-2,4-$C_2B_4H_4$ (**VI**) with thermal ellipsoids drawn at the 40% probability level and showing the atom numbering scheme. The $SiMe_3$ and the (ferrocenylmethyl)-*N*,*N*-dimethylamine H's are omitted for clarity.

In each base–stannacarborane complex the tin, in a formal oxidation state of +2, occupies the apical position above the C_2B_3 open face of the carborane and is bonded to the nitrogen atoms of the particular Lewis base. The C_2B_3 faces are essentially planar (see Table 4), with the structures giving no hint of the ring folding that is commonly found in the carbons adjacent metallacarboranes.[3–6] The base molecules do not occupy the sterically preferred positions directly opposite the carborane ligands, but are oriented to one side of the carborane. The tin atoms are not equally bonded to the C_2B_3 atoms of the carborane faces, but are slightly dislocated, or slipped, toward the direction of base orientation. For example, in **III** the bipyridine is oriented opposite the unique boron atom in the C_2B_3 face, B(2) in Figure 1, and the Sn–B(2) bond is noticeably longer than the Sn–B(4,5) distances (the relevant distances are Sn–B(2) = 2.683 Å, Sn–B(4) = 2.393 Å, and Sn–B(5) = 2.405 Å; see Table 3). A comparison of the Sn–B(2), Sn–C(3), and Sn–B(4) bond lengths with the Sn–C(1) and Sn–B(5) distances in **IV**, and the Sn–B(2) and Sn–C(3) with the Sn–B(4), Sn–B(5), and Sn–C(1) bond lengths in **VI**, shows similar, but smaller, distortions (see Table 3). Slippage of the capping metal in the direction of base orientation

Table 7. Calculated Values of ΔH for Some "*Carbons Apart*"–"*Carbons Adjacent*" Interchange Reactions

reaction[a]	ΔH (kJ/mol)
$[2,3\text{-}C_2B_4]^{2-} \rightarrow [2,4\text{-}C_2B_4]^{2-}$	−118
1-Sn-2,3-C_2B_4 + $[2,4\text{-}C_2B_4]^{2-} \rightarrow$ $[2,3\text{-}C_2B_4]^{2-}$ + 1-Sn-2,4-C_2B_4	−6
1-(BP)Sn-2,3-C_2B_4 + 1-Sn-2,4-$C_2B_4 \rightarrow$ 1-Sn-2,3-C_2B_4 + 1-(BP)Sn-2,4-C_2B_4	33

[a] 2,3-C_2B_4 = 2,3-$(SiMe_3)_2$-2,3-$C_2B_4H_4$, 2,4-C_2B_4 = 2,4-$(SiMe_3)_2$-2,4-$C_2B_4H_4$, and BP = 2,2′-bipyridine ($C_{10}H_8N_2$).

is a common feature found in the donor–acceptor complexes of the pentagonal bipyramidal and icosahedral carbons adjacent main group metallacarboranes; however, their structures are more regular in that in most of these complexes the base is oriented over the unique boron of the C_2B_3 bonding face, which results in slippage toward the boron side of the bonding face.[1,2] In general, the slip distortions found in **III**, **IV**, and **VI** are smaller than those found in their respective carbons adjacent analogues. Because of the different directions of metal slippage and the permutations of the carbon and boron atoms of the C_2B_3 bonding faces, an atom-by-atom comparison of the tin–carborane bond distances in the two carborane systems is not particularly useful. However, the shortest Sn–B bond distance in the carbons adjacent bipyridine–stannacarborane complexes was found to be 2.37 Å,[3b] which is not too different from the Sn–B(4) and Sn–B(5) distances of 2.405 and 2.393 Å, respectively, found in **III** (see Table 3). While the tin–carborane distances in the two isomers are comparable, the Sn–N distances of 2.614 and 2.625 Å, shown in Table 3 for compound **III**, are considerably longer than the values of 2.49 and 2.54 Å found for its carbons adjacent isomer.[3b] Inspection of Table 4 shows that the dihedral angle between the molecular plane of the bipyridine and the C_2B_3 carborane face is 33.3°, which is larger than the value of 21° found for its carbons adjacent isomer.[3b,i] The larger base–carborane dihedral angle, coupled with the longer Sn–N bonds, indicate weaker base–tin bonding.[20a] The Sn–N bond distances in **IV** and **VI** are also longer than those found in their respective carbons adjacent isomers,[3f] indicating weaker base–metallacarborane bonding. Although the relative base binding abilities of the carbons apart and carbons adjacent stannacarboranes have not been studied experimentally by direct competitive reactions, they can be probed theoretically. Table 7 lists the values of the ΔH's for a series of interchange reactions obtained from the MNDO calculated values of the ΔH_f's of the involved species.[29] The ΔH's indicate that, while the carbons apart dianion is considerably more stable than its carbons adjacent isomer, the two dianions bond equally well with tin. However, the carbons adjacent stannacarborane seems to be a stronger Lewis acid than is **I**. These results are consistent with the experimental results found in this study.

The geometries of adducts **IV** and **VI**, shown in Figures 2 and 3, are much less symmetric than that of **III**. The Sn–N(20) and Sn–N(13) bond distances in **IV** are 2.832 and 2.640 Å, respectively, indicating much stronger bonding to one of two equivalent nitrogens (see Table 3). This unequal bonding is also reflected in the dihedral angle of 9.5° between the two pyrimidine rings of the base (see Table 4). The midpoint of the bipyrimidine base [the C(18)–C(19) midpoint in Figure 1] does not reside on the pseudomirror plane of the carborane cage, but is twisted by an angle of 55.6°, so that it resides over atoms C(3) and B(4), with the shorter Sn–N bond being closer to B(4); see Figure 2. Given the almost 0.2 Å difference in the two Sn–N distances, one could just as well describe the base as a monodentate, rather than bidentate, ligand. This is quite different from the situation found for the carbons adjacent bipyrimidine–stannacarborane complex, where two stannacarboranes were equally bonded to the adjacent nitrogens on each side of the bipyrimidine, giving a bridged complex in which the base acts as a bis(bidentate) ligand.[3g] The shorter Sn–N bond distance of 2.640 Å in **IV** is essentially the same as the Sn–N distances of 2.638 Å found in the carbons adjacent bridged complex.[3g] At present there is no ready explanation for the unequal bonding and base orientation found in **IV**. Given that **I** is a weaker Lewis acid than its respective carbons adjacent analogue and that bipyrimidine is a weaker donor than bipyridine, the asymmetry found in **IV** most probably arises from external (crystal packing) forces acting on a relatively shallow and broad potential energy surface, rather than from strong bonding preferences within the molecule. The unusually broad ^{11}B NMR resonances found in the base–stannacarborane adducts, **IV**–**VIII**, could reflect some nonrigidity in the solution structures of these adducts, which would indicate a rather broad energy potential governing the placement of the base.

In the ferrocene amine complex, **VI**, the Sn–N bond does not reside in the pseudomirror plane of the carborane cage, but is oriented almost directly over one of the basal borons, B(4) in Figure 3 (the Sn–N bond is rotated out of the plane by 41°, compared to 39° for the Sn–B(4) bond). The Sn–N bond distance of 2.723 Å in **VI** is substantially longer than the value of 2.557 Å reported for its carbons adjacent analogue,[3f] indicating weaker tin–base bonding, as was the case found for the two other bases used in the present study. At the Fenske–Hall level of analysis, no reason could be found for preferring this orientation over one in which the base nitrogen is in the SnC_2B_4 mirror plane. Given the weaker base bonding and the broadness of its solution ^{11}B NMR spectra, the structure of **VI**, shown in Figure 3, could represent only one of several different, nearly energy equivalent, structures that could exist for this complex in solution. It is of interest to note that the ferrocenyl group in **VI** is rotated away from the stannacarborane moiety so that there is essentially no direct interaction between the tin and the ferrocene group (see Figure 3). This is quite different from the situation found in the analogous carbons adjacent ferrocene amine–group 14 metallacarborane complexes. In all of these adducts the ferrocenyl group was rotated so that there was a direct interaction between the group 14 metal orbitals and several of the cyclopentadienyl carbon π orbitals of the ferrocene. It was suggested that the small stabilizing effect of such interactions helped stabilize the nonsterically preferred ferrocene orientation.[5b] In **VI** the added repulsion due to the nearer presence of the Me_3Si–C_{cage} groups resulting from a closer ferrocene–tin distance would be more than enough to overcome any stabilizing effect that might result from direct tin–Cp interactions so that the structure shown in Figure 3 would be the expected lowest energy one.

(29) Selected interatomic distances calculated for **III** are listed in Supplementary Table S-4. MNDO underestimates the Sn–C_2B_3 ring atom distances by about 0.11 Å; the other calculated intercage distances agree with experiment to be better than 0.01 Å. A similar comparison of calculated and experimental bond distances in the "*carbons adjacent*" isomers is given in ref 20.

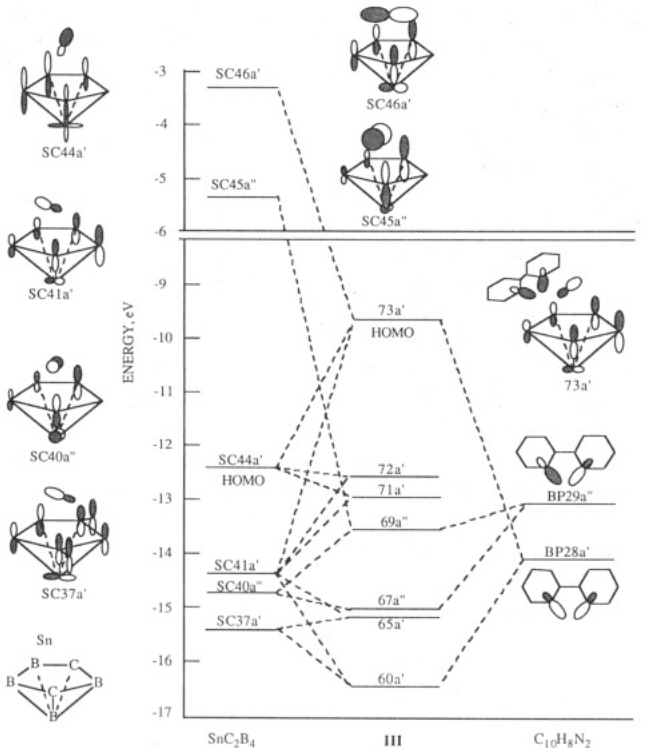

Figure 4. Molecular orbital correlation diagram for **III** in terms of its stannacarborane and bipyridine fragments and sketches of some associated orbitals.

Some of the general structural and bonding features of **III**, and to lesser extents, **IV** and **VI**, can be understood by considering Figure 4, which shows the molecular orbital correlation diagram for **III**, in terms of its stannacarborane and bipyridine fragments, obtained from Fenske–Hall calculations. Also shown in the figure are sketches of some of the more important fragment and adduct molecular orbitals (MO). In the calculations, a coordinate system was defined such that the mirror plane of the $(C_{10}H_8N_2)$-SnC_2B_4 atom network was taken as the xz plane, with the unique boron, B(2) in Figure 1, being placed on the x axis; the symmetry notations of the orbitals in Figure 4 are with respect to that mirror plane. The correlation diagram shows that the bipyridine bonds to the stannacarborane through the interactions of bipyridine fragment orbitals BP28a′ and BP29a″, the respective symmetric and antisymmetric base "lone pair" orbitals, and a set of high energy tin containing metallacarborane orbitals. It is also apparent from this diagram that the base and the carborane ligands compete for the same tin orbitals, so that tin–bipyridine bonding will be at the expense of tin–carborane bonding. The percent atomic orbital compositions of the molecular orbitals of **III** and its stannacarborane fragment are given in Supplementary Tables S-4 and S-5, respectively. The correlation diagram shows that the main bipyridine–stannacaborane interactions take place through MO's 73a′, 67a″, and 60a′. The strongest base–metallacarborane bonding is through MO's 67a″ (54% SC40a″ and 29% BP29a″) and 60a′ (6% SC41a′, 21% SC37a′, and 39% BP28a′). Molecular orbital 73a′ (23% SC46a′, 33% SC44a′, 15% SC41a′, and 17% BP28a′) contributes to both tin–base bonding and tin slip distortion (see Figure 4). The lowest energy vacant symmetric stannacarborane fragment orbital, SC46a′, which is heavily localized on Sn (52% $5p_x$ and 5% $5p_z$) and each of the cage carbons (10% p_z) in an antibonding configuration, contributes substantially, 23%, to the composition of MO 73a′, which results in a strong antibonding interaction arising between the tin and those atoms in the carborane face opposite to the base [C(1), B(2), C(3) in Figure 1].[30] Although MO 69a″ is composed of a good mixture of PB29a″ (29%) and stannacarborane fragment orbitals (5% SC45a″, 27% SC42a″, 26% SC40a″, and 11% SC36a″), the resulting MO has essentially no tin character and therefore does not play a significant role in either tin–carborane bonding or metal slip distortion. Although analyses such as these are useful in that they show that base coordination preferentially weakens the tin–carborane atom bonds that are *trans* to the base, they offer only limited insight into the various competing bonding interactions that cause, and limit, metal slip distortion. These can be better understood from Table 8 that gives the one-center and two-center energy terms calculated by MNDO for the different atom–atom interactions in **I** and **III** as functions of Δ, which is the lateral displacement of the tin atom, in Å, from the extension of the normal line drawn from B(6) to the C_2B_3 plane of the carborane; a positive value of Δ indicates a displacement toward the unique boron, B(2), while a negative value means displacement toward the B(4)–B(5) midpoint (see Figure 1).[31] In these calculations the positions of the C_2B_4 carborane cage atoms were fixed at the experimental values of **III**; under these constraints the optimized value of Δ was −0.46 Å and the bipyridine–C_2B_3 dihedral angle was 43.7°, compared with the experimental values of −0.37 Å and 33.3°, respectively. In the calculations summarized in Table 8, the Sn–N bonds were fixed at their optimized positions; when the Sn–N distances were allowed to optimize, the calculations showed that a tin–bipyridine bond cleavage occurs when Δ became more positive than 0.001 Å. Similar calculations on the carbons adjacent isomer did not show a tin–base, or a tin–carborane, bond rupture at comparable values of Δ, which again points to **I** and **II** being fairly weak Lewis acids. Table 8 shows that the tin position above the C_2B_3 face is determined by a number of competing energy changes. In both the stannacarborane and its bipyridine adduct, tin–carborane bonding, as measured by the two-center energy terms, increases as the tin moves toward the cage carbons rather than toward the borons; however, this increased bonding is at the expense of other intracage bonding interactions, especially those involving the cage carbons and their neighboring borons. The net result is an optimized structure in which the tin is slightly slipped away from the unique boron and cage carbon atoms. Table 8 shows that as the tin atom in **III** moves away from the unique boron, tin–bipyridine bonding increases and the bipyridine molecule tends to align itself more parallel with the C_2B_3 carborane face. The importance of the base–carborane dihedral angle to the overall stability of the complex can be seen in Figure 5, which shows a plot of the energy of **III**, measured as ΔH_f, as a function of this dihedral angle. Also shown in the figure is a similar plot when the Sn^{2+} is replaced by a purely ionic divalent cation. A dihedral angle of zero corresponds to the bipyridine and

(30) Preferential bond weakening is also reflected by the change in the overlap populations before and after base coordination; the Sn–B(4,5), –C(1,3), –B(2) overlap populations for **III** are 0.2861, 0.0836, and 0.0732, respectively, compared to values of 0.3087, 0.1855, and 0.2300, respectively, for its stannacarborane fragment.

(31) Δ gives the displacement of the metal compared to the apical boron; a value of Δ = 0 does not imply equivalent bonding to the C_2B_3 ring atoms. For comparison, the Δ's for the B(2), C(1,3), and B(4,5) atoms in **III** are +1.196, +0.272, and −1.261 Å, respectively.

Table 8. One-Center and Two-Center Energy Terms Calculated for I and III as a Function of Δ[a]

			1-Sn-2,4-$(SiMe_3)_2$-2,4-$C_2B_4H_4$			
Δ, Å	−0.883	−0.511	−0.223[b]	−0.007	0.342	0.532
$\sum E_{AB}$(CB)[c] eV	−452.422	−451.874	−451.483	−451.221	−450.872	−450.728
$\sum E_{AB}$(Sn–CB), eV	−18.477	−19.233	−19.588	−19.596	−19.221	−18.931
$\sum E_A$(CB), eV	−1333.539	−1333.298	−1333.250	−1333.341	−1333.699	−1333.964
E_A(Sn), eV	−83.090	−83.707	−83.982	−84.027	−83.794	−83.527
E, eV	−1887.528	−1888.112	−1888.303	−1888.185	−1887.586	−1887.150
			1-$(C_{10}H_8N_2)$Sn-2,4-$(SiMe_3)_2$-2,4-$C_2B_4H_4$			
Δ, Å	−0.932	−0.724	−0.456[b]	0.001	0.366	0.571
$\sum E_{AB}$(CB), eV	−453.513	−453.273	−452.900	−452.160	−451.604	−451.361
$\sum E_{AB}$(BP)[c] eV	−344.033	−344.031	−344.012	−343.961	−343.922	−343.914
$\sum E_{AB}$(Sn–CB), eV	−15.421	−15.861	−16.402	−16.863	−16.850	−16.754
$\sum E_{AB}$(Sn–BP), eV	−5.447	−5.122	−4.716	−4.242	−4.234	−4.494
$\sum E_{AB}$(CB–BP), eV	−0.120	−0.070	−0.010	0.050	0.089	0.093
$\sum E_A$(CB), eV	−1334.700	−1334.551	−1334.421	−1334.538	−1334.970	−1335.312
$\sum E_A$(BP), eV	−1455.780	−1456.022	−1456.325	−1456.693	−1456.724	−1456.526
E_A(Sn), eV	−83.373	−83.555	−83.786	−83.806	−83.276	−82.797
E, eV	−3692.387	−3692.485	−3692.572	−3692.213	−3691.491	−3691.065
BP–CB angle,[d] deg	29.74	36.28	43.66	52.22	50.62	48.54

[a] Carborane cage atoms fixed at the experimental positions of III; for reference, Δ[B(4,5)] = −1.261 Å, Δ[C(1,3)] = 0.272 Å, and Δ[B(2)] = 1.196 Å. [b] Optimized value. [c] CB = 2,4-$(SiMe_3)_2$-2,4-$C_2B_4H_4$, BP = 2,2′-bipyridine, $C_{10}H_8N_2$. [d] Dihedral angle between the plane of the $C_{10}H_8N_2$ and the carborane C_2B_3 face.

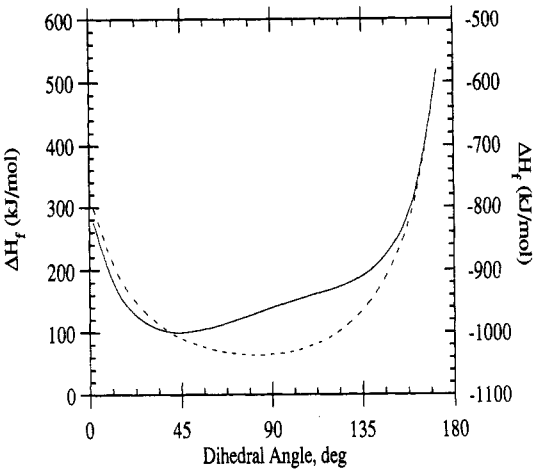

Figure 5. ΔH_f of 1-$(C_{10}H_8N_2)$E-2,4-$(SiMe_3)_2$-2,4-$C_2B_4H_4$ as a function of the base-carborane dihedral angle: (solid line) E = Sn, left-hand scale; (dashed line) E = M (a purely ionic divalent cation), right-hand coordinate.

carborane face being parallel with the base oriented over atoms B(4) and B(5), while 180° corresponds to a parallel alignment with the base oriented over B(2). In these calculations the SnC_2B_4 geometry and the tin–bipyridine distances were fixed at their optimized values. The plot shows a minimum at the optimized angle of 44°, with an inflection point occurring at about 120°. The calculations show that tin–bipyridine bonding is accomplished mainly through the interaction of the base nitrogen lone pairs and the two tangentially directed tin p orbitals, the Sn-($5p_x$) and Sn($5p_y$) orbitals in the present coordinate system. Overlap would be at a maximum when the plane of the bipyridine and the carborane bonding face are aligned parallel to one another; however, repulsion between the two ligands prevents this preferred arrangement. An increase in slip distortion would decrease the ligand–ligand repulsion, allowing a more parallel arrangement, resulting in stronger base bonding, even at the expense of tin–carborane bonding. Thus, the driving force for the increased slip distortion on complexation of the stannacarborane with a base, is the relief of ligand–ligand repulsion, thereby allowing enhanced base–metal bonding. Such slippage is aided by the weakening of tin bonding to the carborane atoms opposite the base, but this does not provide the driving force for the structural distortions found in the base–stannacarborane complexes. In general, one would expect weaker base–tin bonding to be reflected, not only in longer base–metal bonds but also in smaller slip distortions and larger base–carborane dihedral angles. The weaker bonding in the carbons apart stannacarborane–Lewis base complexes found in the present study reflects those structural tendencies.

Acknowledgment. This work was supported by grants from the National Science Foundation (CHE-9100048), the Robert A. Welch Foundation (N-1016), and the donors of the Petroleum Research Fund, administered by the American Chemical Society. We thank Dr. Anil Saxena for his help in preparing the initial draft of the manuscript.

Supplementary Material Available: Tables of anisotropic displacement parameters (Table S-1), H atom coordinates and isotropic displacement coefficients (Table S-2) for **III**, **IV**, and **VI**, MNDO optimized bond distances in **III** (Table S-3), and compositions of the molecular orbitals of **III** (Table S-4) and its stannacarborane fragment (Table S-5) and a figure showing the atom numbering scheme for Tables S-4 and S-5 (35 pages). Ordering information is given on any current masthead page.

OM930833G